Recent advances on the structure–properties relationship of multiblock copolymers

Guilhem P. Baeza

Recent Advances on the Structure-Properties Relationship of Multiblock Copolymers

Guilhem P. Baeza

Univ. Lyon, INSA-Lyon, CNRS, MATEIS, UMR 5510, 7 Av. Jean Capelle, 69621 Villeurbanne, FRANCE

Dated: September 19, 2021

ABSTRACT: Multiblock copolymers represent a fascinating class of materials that sits at the very heart of industrial applications and fundamental polymer science. They are most often made of a linear succession of incompatible "soft" and "hard" segments that microphase separate at room temperature while they can be easily re-homogeneized upon heating. This thermoreversible character provides them with decisive advantages with respect to other rubber-based materials such as vulcanized elastomers, making them indispensable for the development of a more sustainable polymer industry. Beyond practical opportunities, tailoring the multiblock copolymers morphology has a pivotal role to play in the fundamental understanding of the structure-properties relationship of polymer-based systems. It notably serves to comprehend complex materials such as semi-crystalline homopolymers and nanocomposites. Aside from the thorough work developed on well-defined diblock copolymers for half a century, this article review aims to guide the reader into the more intricate world of multiblock copolymers by providing him/her quantitative tools to connect chemical nature, microstructure and mechanical properties.

Keywords: multiblock copolymers, segmented copolymers, thermoplastic elastomers, phase separation, rubber elasticity, crystallization

Contents

1 Introduction

In 2012, Bates et al. wondered in a short review article whether multiblock copolymers should be seen as Panacea or Pandora's box,[1] suggesting great possibilities accompanied with an evident lack of knowledge on this seemingly infinite field of research. In fact, varying the number (n) and type (k) of blocks within these molecules, together with an appropriate tailoring of the molecular architecture, could result in an unlimited range of morphologies and physical properties.

The present review focuses on the sub-ensemble of multiblock copolymers (denoted MBCs hereafter) satisfying $n \geq 3$ and $k = 2$, *i.e.*, molecules of type -$(AB)_x$-A (with $x \geq 1$), excluding *de facto*, thoroughly studied diblock copolymers and any sort of terpolymers, *e.g.*, -$(ABC)_x$- like structure. It also includes triblock copolymers of type B-A-B and, occasionally, other architectures such as bottlebrush and star copolymers. The peculiar case of ring copolymers is also evoked. What makes MBCs fundamentally different from diblock copolymers stems in their ability to form "loop" and/or "tie" segments resulting in complex network topologies. In the context of this review, "loops" and "tie" refer to A-blocks connected covalently twice to the same B-domain, and bridging two distinct B-domains, respectively.

A-blocks most often refer to apolar "soft" segments (SSs) made of a low-T_g polymer such as polybutadiene (PB),[2–4] polyisoprene (PI),[5–9] polyethylene oxide (PEO),[10, 11] polyethylene (PE),[12, 13] polypropylene (PP),[14] polydimethylsiloxane (PDMS),[15, 16], poly-1-octene,[17] or the popular polytetrahydrofuran (PTHF),[18–28] providing the material with its flexibility. While some of the above-mentioned SS have the possibility to crystallize (*e.g.*, above 2 $kg\ mol^{-1}$ for PTHF), they are mostly amorphous at service temperature and at rest. On the other hand, B-blocks are generally made of a polar and high-T_g polymer, also called "hard" segments (HSs), which associate at low temperature resulting in the formation of a physical network ensuring the elasticity of the MBC. Common crystallizable B-blocks, which often give rise to long ribbon-like crystallites, are mainly based on polyesters, like polybutylene terephthalate (PBT)[18–21] and polyethylene terephthalate (PET),[11] or polyamide, like T4T,[22, 23, 29], T6T,[24] T6A6T,[25] T6T6T,[30]

TΦT,[26, 27] oxalamide,[31] PA12[28] and PA1012[32] among others. Besides, thermoplastic polyurethanes (TPUs), based on diisocyanate HSs, are appreciated for their great chemical tunability, involving either crystalline or amorphous hard domains.[33–36]. In this case, the word "ordered" is sometimes used to substitute "crystalline",[37] revealing the uncertainty regarding the molecular arrangement of these complex molecules.[38–41] Lastly, polystyrene (PS) forming amorphous spherical domains in soft PB or PI is used for several decades,[2–8] and until recently, in association with soft poly(phenylene sulfide sulfone).[42] Note that beyond their chemical nature, their length and their number density, the HSs polymolecularity, their position in the chain and the architecture of the molecule (*e.g.*, comb, stars ...) strongly impact the phase diagram of MBCs.[43–46]

The interest of MBCs is multiple. On one hand, it concerns industrial applications, where MBCs are mainly used as thermoplastic elastomers (TPEs) for which the 3.84 millions tons market in 2021 is expected to grow to 5.55 millions tons by 2026.[47] These materials present the great advantage to be melt processable and possibly reparable on-demand,[48, 49] making them promising candidates to substitute vulcanized rubbers in many applications including, but not limited to, wire sheaths,[50] shoe soles, seals and possibly tires.[51, 52] Besides, TPEs are frequently used as bitumen modifiers,[53, 54] adhesives,[55, 56] energy dissipators,[57] reinforcing fibers,[58] ground coverings, polyelectrolytes,[42, 59] compatibilizers,[60] strain sensors,[61, 62] antibacterial coatings[63] and particularly in the car industry as dashboard elements or other automotive parts.[64, 65] On top of this, MBCs progressively become eco-friendly, incorporating bio-degradable HSs,[66, 67] without significant loss of mechanical properties.[68] This great variety comes from continuous progress in chemistry, making it possible to modify on-demand the number of segments, their length and the polymers architecture,[69] resulting in a wide range of accessible microstructures. Beyond their applications as bulk materials, it is worth noting that their association with an appropriate solvent can result in astonishing self-assembled structures serving as drug deliverers,[70] cameleon-like skin,[15], or spatio-temporal reversible networks.[71]

On the other hand, MBCs provide an unique opportunity to investigate more fundamental aspects of polymer physics and biology. They may be seen as the missing link between

well-known diblock copolymers and extremely complex semi-crystalline homopolymers or proteins. On one side, diblock copolymers were extensively studied from both experimental[43] and theoretical points of view,[72, 73] enabling major advances in their understanding and utilization. On the other side, semi-crystalline homopolymers, apparently simpler from a chemical point of view (*e.g.*, PE), give rise to an intricate multiscale structuration (chain-lamella-spherulite)[74] from which properties prediction still remains vague after a century of polymer science.[75] One can however note the recent breakthrough in solving proteins structure made possible thanks to artificial intelligence,[76] a highly valuable tool that will support, if not guide, physico-chemical characterizations in the future.

Focusing now our attention on the MBCs' literature reveals that much less effort have been made to rationalize their structure-properties relationship. In fact, while a large amount of research articles have been published in the field for more than 50 years, it appears that the large variety of molecular chemistries and architectures have somehow discouraged the community from building theoretical models aiming to bridge MBCs' microstructure with their physical behavior. In other words, in spite of a growing number of available methods of characterization, a great part of the knowledge on MBCs remains empirical. A few exceptions are nevertheless worth to mention, starting from the analytical model proposed by Krause in the 70's[77] to the continuous development of the self-consistent field theory (SCFT) in the 90's[78, 79] until its most recent advances[80, 81](see section 2.1).

The most typical investigation on MBCs consists of increasing the fraction of crystallizable HSs in a polymer and measuring its growing melting point (T_m)[22] and/or elastic modulus (E)[82] and/or stress at failure[83] (σ_{max}). While these results are qualitatively expected from the larger size of crystallites and content in hard phase, little is known on the impact of non-chemistry oriented variables such as the network topology, on both T_m and E. However, we believe that a deeper and more general understanding is possible. In fact, while MBCs look more complicated than semi-crystalline homopolymers for a chemist, it is the opposite for a materials physicist that can picture them as molecules in which crystallizable repetition units are pre-identified, reducing therefore the number of accessible configurations. In addition, the democratization of numerical simulations based on SCFT[80] or molecular

dynamics, providing the position of all the atoms (or "coarse grains"[84, 85]) at any time, gives hope for the coming years.

MBCs not only are at the crossroads of diblock copolymers and semi-crystalline homopolymers. Recent studies indicate that they could also be understood from the relatively recent formalism of supramolecular polymers.[86] Indeed, reducing the length[29] or the probability to crystallize of the HSs (either chemically[87] or thermally[88]) results in a situation comparable to a polymer chain carrying punctual "stickers", *i.e.*, chemical moieties able to associate to form dimers[89] or more complex thermoreversible structures.[90] This analogy makes it possible to further decrease the degree of complexity of MBCs with the aim to better comprehend their network topology serving as a basis to rationalize their structure-properties relationship. This philosophy, which appears particularly promising, is at the heart of the section 3.

2 About the structure

2.1 Elements of theory: on the microphase separation

In the early 40's, Flory and Huggins developed a theory applicable to polymer melt mixtures to determine the free energy of mixing of a binary system where they quantified the interactions between chemical species (A and B) through a single variable, now known as the Flory-Huggins parameter, as follows[91, 92]

$$\chi_{AB} = \frac{z}{k_B T}\left(\frac{1}{2}(E_{AA} + E_{BB}) - E_{AB}\right). \tag{1}$$

E_{ij} refers to the interaction energy between i and j units, z is the number of nearest neighbors, k_B is the Boltzmann's constant and T is the temperature. Another popular and more chemistry-oriented formulation based on the Hildebrandt solubility parameter (δ_i in $(J/m^3)^{1/2}$) was also proposed,

$$\chi_{AB} = V_{ref} \times \frac{(\delta_A - \delta_B)^2}{RT} \tag{2}$$

where V_{ref} is the reference (molar) volume and R is the perfect gas constant. Here, the solu-

bility parameter can be further dissociated into three components standing for the dispersive δ_D, polar δ_P and hydrogen bonds δ_H interactions such as:

$$\delta = \sqrt{(\delta_D^2 + \delta_P^2 + \delta_H^2)} \tag{3}$$

Whatever the field of research, χ_{AB} is used to quantify the free energy cost of contact between A and B units. While its magnitude describes the amplitude of the interaction, its sign indicates whether it is attractive (-) or repulsive (+). Note that although most polymer-pairs are repulsive, increasing the temperature favors their compatibility.

Beyond enthalpic interactions, phase separation occurring in bicomponent polymers strongly depends on the difference of accessible chain conformations in ordered and disordered states. In fact, phase-separation requires the chain to adopt particular conformations reducing their entropy, *i.e.*, creating a force that limits the phase separation. A stable microstructure eventually emerges when enthalpic and entropic interactions balance each other.

After several decades of theoretical development,[93, 94] the Flory-Huggins theory was extended in the early 80's by Leibler to diblock copolymers,[72] predicting a wide variety of microstructures (spherical, rod-like, gyroid and lamellar phases) according to the χ_{AB} value, the polymer length and the relative fractions of A and B units. From the late 80's and during the 90's, experimental and theoretical works of Matsen[73], Fredrickson[95, 96] and Bates[97, 98] further improved the understanding of the phase separation process and resulting microstructures for amorphous di- and tri-block copolymers. Models that adress more complex polymer architectures, like *e.g.*, comb-shaped triblock copolymers,[99] are still in development today, evidencing the vitality of this research field.

The situation becomes however more intricate when increasing the number of blocks within the chain. While some theoretical investigations have shown that amorphous MBCs can present similar microstructure as their diblock counterparts,[44, 73] structural characterizations unambiguously showed that the number of blocks within the chain can be used to tune both the microstructure and the order-disorder transition temperature.[100–102] Here, an important issue is that the number of blocks n is not independent of the molecular weight of the polymer M, hard-segment M_{HS} and soft-segment M_{SS}, $[n = (M - M_{SS})/(M_{SS} + M_{HS})]$,

making its variation analysis non-straightforward. Prior to the seminal work of Leibler, Krause proposed in the late 70's a "zeroth approximation" model adapted from the Flory-Huggins' theory to treat the case of MBCs. She notably formalized the (covalent) junction of two consecutive blocks as well as their number within the chain, resulting in the following prediction for the free energy variation of microphase separation:

$$\frac{\Delta G_{Krause}}{k_B T} = -N_r \nu_A \nu_B \chi_{AB} \left(1 - \frac{2}{z}\right) - N_0 ln(\nu_A^{\nu_A} \nu_B^{\nu_B}) + 2N_0(n-1)\frac{\Delta S_{dis}}{k_B} - N_0 ln(n-1) \quad (4)$$

where N_r is the total number of units (lattice theory of polymers), ν_A and ν_B are the respective fractions in A and B units, N_0 is the number of chains and ΔS_{dis} is the entropy loss corresponding to a segment immobilization that can be evaluated through:

$$\Delta S_{dis} = k_B(ln(z-1) - 1). \quad (5)$$

Although this model is not space-resolved, *i.e.*, it does not predict any particular morphology, it enables the calculation of the order-disorder temperature corresponding to a negative variation of ΔG_{Krause}. Also, it well captures the fact that a higher number of blocks increases the demixing free energy, reducing the tendency of the copolymer to phase separate at a given temperature. The two extreme situations arise for diblock copolymers in which phase separation is promoted, and for statistical copolymers in which blocks are made of a single repetition unit, inhibiting any phase separation.

Since the late 90's, polymer-oriented SCFT coupled with numerical resolution methods have emerged as the state-of-the-art technique to predict the structure of multiphasic polymer-based systems, including MBCs.[78, 80, 81, 103, 104] In a paper published in 2016, Arora et al. notably invite polymer physicists to utilize more SCFT to design their experiments, similarly as what is done in fluid mechanics or quantum chemistry with similar computationnal tools.[80] In the present context, SCFT consists of reducing the many-body problem describing the thermodynamics of a polymer melt into an easier problem of analyzing the conformation of a single chain in a potential field created by the other chains. Because they do not require to simulate every monomers, they are much less expensive than compet-

ing particle-based methods such as coarse-grain molecular dynamics simulations (CGMD) and can be used from a modest desktop computer (see section 2.3.2). The configurations of chains are modeled by using random-walk statistics while monomer-monomer interactions are replaced by a monomer interaction with a self-consistently determined chemical potential field. The latter, is defined for every locations ($\mathbf{r}$) and every types of chemical species (A,B,...) in the simulation box, and is related to the Flory-Huggins parameter through

$$\omega_A(\mathbf{r}) = \sum_{B \neq A} \chi_{AB}\ \phi_B(\mathbf{r}) + \xi(\mathbf{r}) \tag{6}$$

where $\omega_A(\mathbf{r})$ is the chemical potential field acting on any monomer A located at a position $\mathbf{r}$, ϕ_B is the local volume fraction of monomer B, and $\xi(\mathbf{r})$ is a Lagrangian pressure field that serves to satisfy the incompressible character of the polymer melt. Note that χ_{AA} is nil, such as defined in Equation 2. Solving a set of equations including Equation 6 then allows to calculate the free energy per monomer similarly as in the above presented models. We refer the interested reader to ref.[80] for comprehensive details regarding polymer-oriented SCFT.

The high complexity, inherent to the architecture of MBCs, becomes even greater when considering the possibility for the SSs and HSs to crystallize at the molecular level. In this case, in addition to the glass transition of each block (T_g^{SS}, Tg^{HS}) and the order-disorder transition, one should consider the crystallization and melting of HSs (and possibly SSs).[105, 106] A common case is that of HSs having a crystallization point (T_c^{HS}) higher than the disorder-order transition temperature. In this situation, the crystallization can occur directly from the homogeneous melt upon cooling, acting as the driving force for the phase separation.[107, 108] Conversely, if T_c^{HS} is lower than the disorder-order transition temperature, the phase-separation occurs first. While other cases may be evoked ($T_g^{SS} > T_c^{HS}$), their interest is limited in the context of this review since it rather focuses on TPE-oriented materials where the transition temperatures must satisfy: $T_g^{SS} < T_c^{SS} < 25°C < T_g^{HS} < T_c^{HS}$.

2.2 Direct probes

The main experimental techniques involved in the direct structural characterization of MBCs rely undoubtedly on microscopy and scattering methods. While microscopy enables a straightforward visualization of microphase separated domains on a limited targeted piece of material, scattering techniques, in which the beam-size is usually far larger than a micrograph dimension, provides more statistical information. Associating both types of techniques enables therefore to be more confident when defining a representative microstructure for a given MBC. In fact, this association is crucial since both microscopy and scattering techniques suffer from drawbacks. In the former, a long and meticulous sample preparation often is required, possibly leading to some surface defects making the material looking different according to the position in the sample. In the latter, the measured intensity $I(q)$ is equivocal. In fact, since a given scattering pattern may correspond to more than one structural configuration, additional sources of information are essential. Also, fitting $I(q)$ with theoretical models to extract structural parameters can be extremely challenging, particularly when dealing with polydisperse (chemistry, size and shape) objects. We refer the reader to the following selection of recent articles in which successful characterizations of MBCs have been obtained through microscopy[15, 54, 70, 109–112] and X-ray scattering techniques.[10, 15, 20, 29, 54, 109, 112–114]. We focus on some of them below.

2.2.1 Microscopy

Popular microscopy techniques used to investigate MBCs are atomic force microscopy (AFM), transmission/scanning electron microscopy (TEM/SEM), and optical microscopy (OM). While the two former probes enable a characterization down to the nanometer lengthscale, relevant to investigate the microphase separation, the latter is mostly used with polarized light to detect wider objects like spherulites above 1 micrometer. In this context, the great advantage of AFM is that it ensures a reasonable contrast between soft- and hard-domains because of different topographic, phase or even mechanical responses.[115] On the other hand, the utilization of SEM and TEM, counting on atomic number variations between the

phases, usually requires staining procedures (*i.e.*, additionnal chemical treatment) to enhance the contrast.

In Figure 1, we have adapted recent works of Nébouy et al.[109] (A-B) and Cao et al.[110] (C-D), highlighting the variety of accessible microstructures in crystallizable MBCs. In the former study, the authors investigate the effect of the processing conditions on the microstructure of commercial MBCs made of PBT HS and PTHF SS. Figure 1A clearly shows the coarsening of the ribbon-like crystallites when passing from drop casting (*1.*) to solvent casting (*2.*) and hot-pressing (*3.*). This effect is mainly assigned to the chains mobility, *i.e.*, to the presence (or absence) of solvent in the environment when the phase separation occurs. These observations are further supported by small-angle X-ray scattering experiments (see Figure 3) confirming the great importance of the processing conditions on the final material's morphology beyond the intrinsic characteristics of the MBC. In the same article, the authors unambiguously show the orthotropic nature of their MBCs by performing AFM not only on the top face of their film but also on their edge (Figure 1B). In fact, long ribbons seen from the top becomes disks when observed in their cross-section (see Figure 1 A*3* vs. B*3*).

Besides, the work of Cao et al., where the authors investigate MBCs made of PA1210 HS and PTHF SS, nicely supports the crucial role of the processing route.[110] Here, the film thickness of spin-coated samples is varied from 200 nm down to 15 nm (Figure 1C*1-3*, respectively), emphasizing the coarsening of the crystallites that is assigned to a lower number of nuclei. Ultimately, when the film reaches ca. 15 nm in thickness, the crystallites growth is strongly reduced due to the confinement effect resulting in a sphere-like morphology (Figure 1C*3*). This study also reveals some interesting changes at the spherulite level, mostly ignored in the MBCs litterature whereas greatly considered in semi-crystalline homopolymers.[74] In fact, the authors show that reducing both the sample thickness and the SS molecular weight (M_{SS} - see Figure 1D) tends to limit the formation of "spherulites with clear boundaries" (Figure 1C*1* and 1D*1*), rather promoting "stacked spherulites" (Figure 1C*2* and 1D*2*) and ultimately, simple lamellae. Note that similar results were obtained by the same group in a slightly older paper [111]. Of potential interest, by following the crystallization kinectics

through DSC, De Almeida et al. found that the formation of spherulites in hot-pressed PBT-PTHF MBCs was most likely happening for SS having a molecular weight lower than 1 $kg\ mol^{-1}$,[116] in good agreement with the present AFM studies.

Two other fascinating MBC based systems with more "exotic" applications are illustrated in Figure 2, adapted from recent works of Vatankhah-Varnosfaderani et al.[15] and Zheng et al.[70]. In the former article, the authors investigate the possibility of active camouflage provided by a triblock copolymer based on PMMA HS and bottlebrush PDMS SS. This material is endowed with extreme softness (apparent Young modulus between 1 kPa and 100 kPa), intense strain stiffening and above all, the ability to change color upon extension, reminiscent of chameleon skin (Figure 2A). The latter property stems in the variation of the distance between hard PMMA domains embedded into the soft PDMS phase, which is further tunable at rest by adjusting the molecular weight of the PMMA blocks. Beyond their utilization as bulk materials, these MBCs can be swollen to form gels of less intense color, being further tunable upon solvent evaporation.

Then, the work of Zheng et al. reported in Figure 2B consists of a structural investigation of self-assembled MBCs in solution, having promising applications as drug deliverer. In this case, the authors' strategy relies on varying the number of blocks to tune the microstructure rather than changing their chemistry (*i.e.*, hydrophilicity). HSs and SSs are respectively made of PCL and PEG, the latter having a greater affinity for water. The structural analysis is performed with TEM rather than AFM because of (i) the need to probe the volume of the material, and (ii) the sufficient contrast offered by the polymer/water couple. When dissolved into water, MBCs self-organize in quite different ways according to the number of blocks within the chains. Isotropic micelles are first obtained for n =2 and n =4 whereas worm-like objects and vesicles emerge for n =10 and n =20 respectively. On top of this, coarse grained dissipative particle dynamics simulations enable a deeper understanding of the MBCs conformation for the whole set of morphologies (see the inset of Figure 2B).

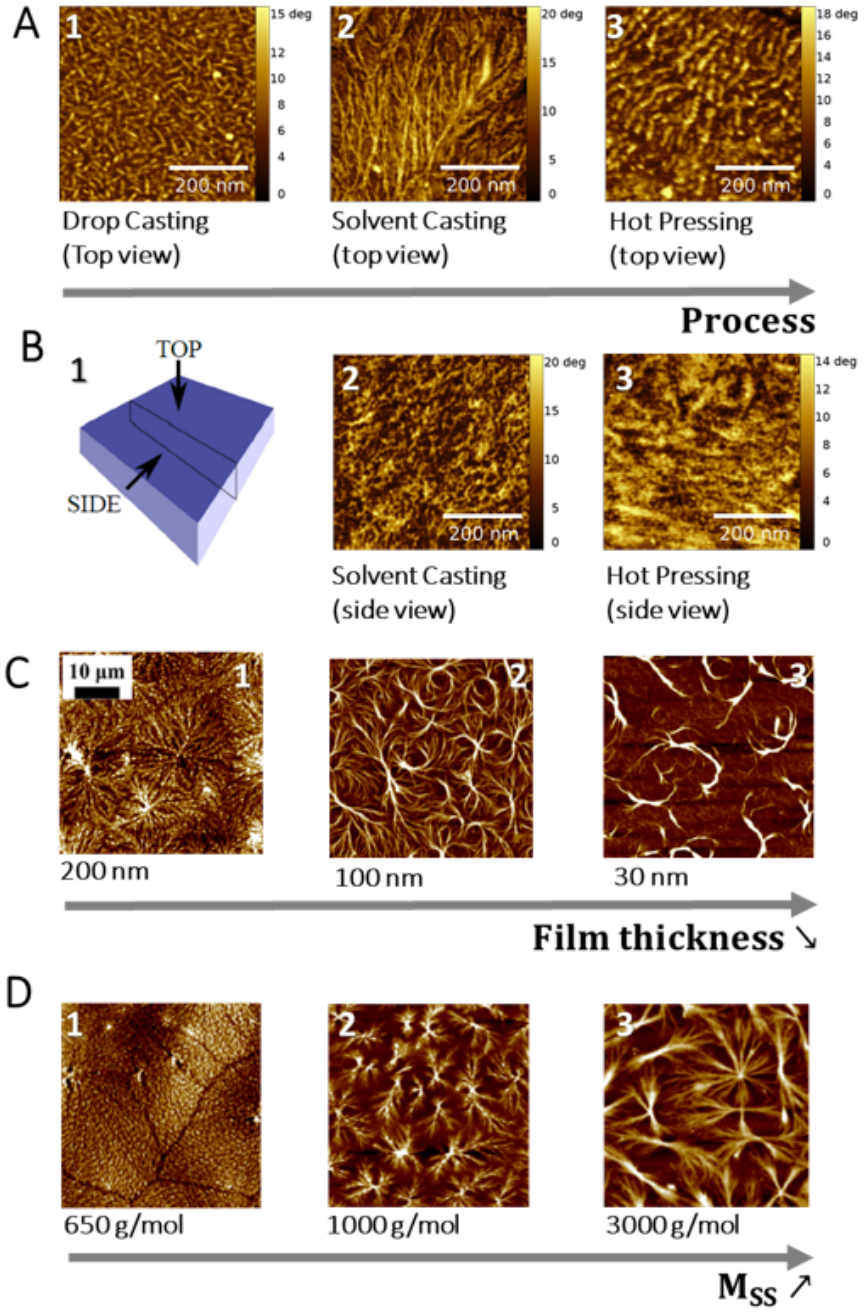

Figure 1: Recent use of Atomic Force Microscopy on MBCs. A) Impact of the processing route on a PBT-PTHF MBC containing 6 HSs per chain in average, adapted from ref.[109]. B) Side views corresponding to A*2.* and A*3.*, adapted from [109]. C) Impact of the film's thickness on the morphology of PA1210-PTHF MBCs, the scale bar is identical in *1.*, *2.* and *3.*, adapted from [110]. D) Impact of the SS molecular weight on analogous MBCs, the scale bar is the same as in C), adapted from ref.[110].

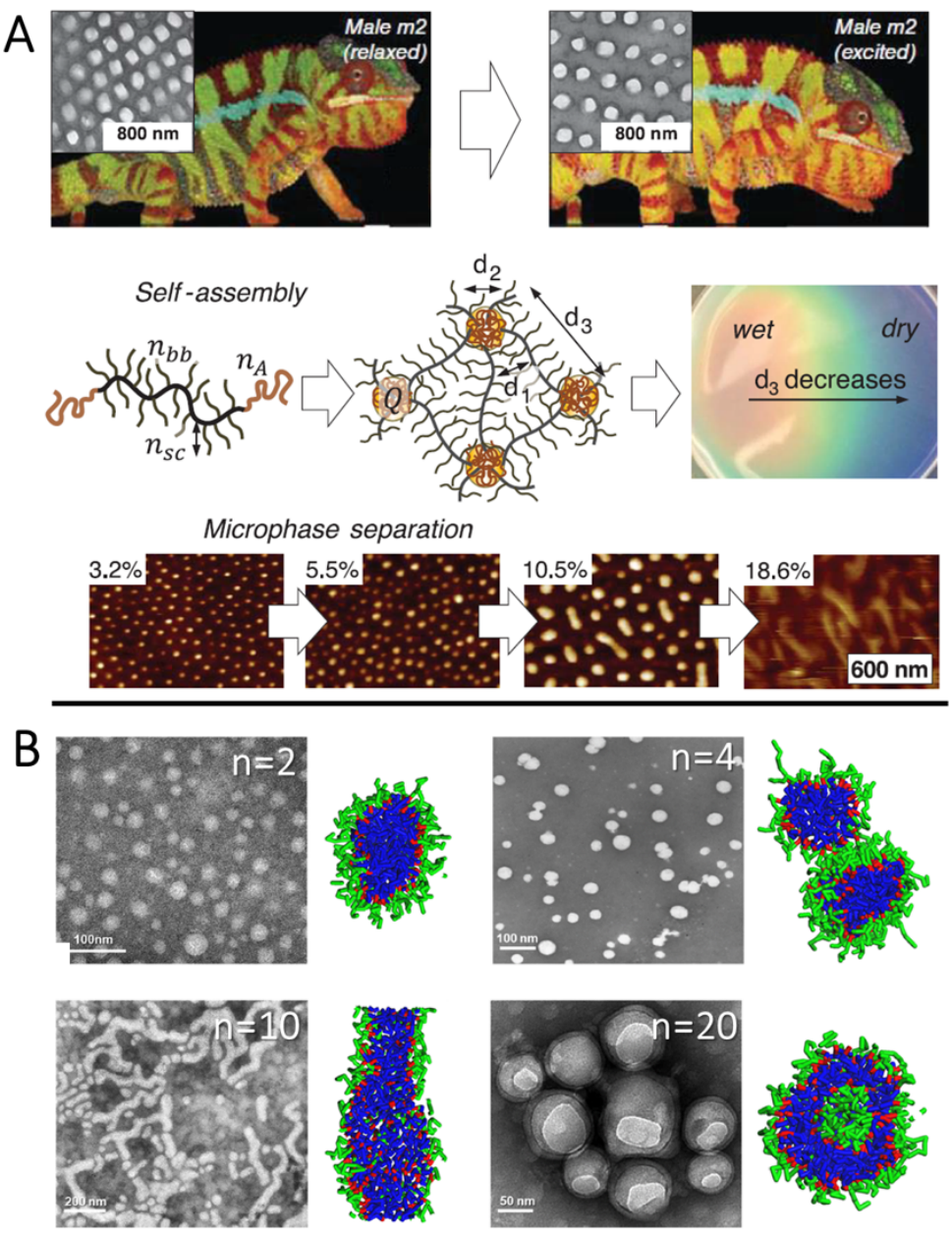

Figure 2: Morpholgy of MBCs used for unconventional applications. A) Top: Chameleon can change color by stretching its skin. Middle: Analogous effect in MBCs made of PMMA HS and bottlebrush PDMS SS both in bulk materials and in gels. Bottom: AFM micrographs of MBCs' microstructure with varying the HS content (and length), adapted from ref.[15]. B) TEM micrographs of MBCs made of PCL HSs and PEG SSs in aqueous solution. MBCs self-assemble in various ways forming isotropic micelles, worm-like objects or vesicles according to the number of blocks n. Insets are corresponding structures obtained from dissipative particle dynamics simulations, adapted from ref.[70].

2.2.2 Scattering methods

The investigation of MBCs' morphology through X-ray scattering mainly rely on small and wide angle X-ray scattering techniques (respectively denoted SAXS and WAXS hereafter). SAXS and WAXS experiments are based on the same principle consisting of irradiating a material with X-rays of typical wavelength 0.5-2.5 Å and measuring the corresponding scattering pattern on a 2D detector located behind the sample. While SAXS (detector-sample distance $>$ 1 m) is used to probe the 0.5-100 nm length scale, WAXS (detector-sample distance $<$ 1 m) provides structural information at 0.1-2 nm, and is particularly used to identify crystalline phases. In addition, ultra-SAXS (detector-sample distance $>$ 10 m), which enables characterization up to the micrometer length scale, is henceforth commonly available at synchrotron sources. When the phase contrast allows it, neutrons scattering is often used as an alternative ("SANS" and "WANS") but usually suffers from a lower incident flux limiting the resolution in time, being yet of great interest to study phase transitions. Graze incidence small angle X-ray scattering (GISAXS), where photons are backscattered, is also growingly used to characterize block copolymers thin films [117–119]; we will however not focus on it in this review. Lastly, the backscattered counterpart of WAXS is usually referred as X-ray diffraction (XRD) by materials scientists studying hard matter in which photons can hardly be transmitted.

In Figure 3, we have gathered SAXS results adapted from refs.[15, 109, 113]. Figure 3A emphasizes the impact of the segmentation degree (*i.e.*, the number of HSs per chain) on the microstructure of MBCs made of EGMEA HSs and tBA SSs. The whole chain molecular weight and the relative fraction in HS and SS are kept unchanged. As one may have anticipated from section 2.1, SAXS reveals a well-defined morphology when dealing with di-block copolymers, as indicated by the sharp structure factor peaks generated by the regularity of the microstructure pattern. More particularly, the emergence of these peaks at q_1=0.027 Å^{-1}, q_2=0.054 Å^{-1}, and q_3=0.081 Å^{-1} indicates the presence of a lamellar phase of long period $d = 2\pi/q_1 = 23nm$.[120] On the contrary, the long range lamellar organization is lost from the tetrablock polymer and higher segmentation degree. In these cases, the X-ray constructive interferences generate a single structure-factor peak that is progressively

shifted to higher q values, indicating a shortening of the characteristic distance between hard domains in agreement with the molecular structure. This is accompanied with a peak broadening synonymous of a lower structural regularity.

Figure 3B then completes the AFM Figure 1A that illustrates the impact of the processing route on the morphology of a PBT-PTHF MBC. In this case, three copolymers containing 30, 40 and 65 wt.% in HS are studied, each of them being prepared through hot-pressing resulting in films of 0.5 and 1.5 mm thickness (for HP^- and HP^+ respectively) or solvent casting (SC) providing the authors with 0.5 mm thick films. Surprisingly, increasing the content in HS, and thus in crystallites (from ca. 5, to 8 and 16 vol.% respectively) does not impact significantly the correlation distance in HP^+ samples, remaining around 40 nm. The situation is slightly different in HP^-, where the HS-richest MBC sees its correlation distance falling down to 21 nm, together with a peak sharpening, indicating a significant improvement in terms of structural regularity. The situation is however very different in solvent-cast samples where a much shorter correlation distance is systematically observed with respect to their HP counterparts. In addition, a clear reduction of the correlation length is observed when increasing the HS content, passing from 15 nm down to 10 nm and 9 nm for 30, 40, and 65 wt.% HS respectively. These results are interpreted by invoking the crystallites' number density. While in HP^+ (and two HP^-) samples, longer HS are believed to form larger crystallites separated by a similar distance, the higher mobility provided by solvent-casting enables the formation of further and narrower objects (making the crystallites fraction identical as in HP samples), resulting inevitably in a shorter distance between their centers of mass. This interpretation was further confirmed by AFM that revealed the presence of thinner ribbons when using solvent-casting (see Figure 1A).

Besides, Figure 3C stands for the SAXS characterization of the above-mentioned PMMA-PDMS triblocks when varying the PMMA length. We believe that it is particularly pertinent here since it illustrates the presence of monodisperse spheres, after lamellae and ribbons reported in the two former studies. The monodisperse character of the PMMA spheres is seen through the form factor oscillations (referred as d_2) that one can compare to the "flat" power law observed in Figure 3B when dealing with ribbons of polydisperse cross-section. In both cases however, the $I \sim q^{-4}$ dependence observed at large $q-$values, indicates smooth inter-

faces between the hard domains and the soft background. Here, the main interest of changing the HS length resides in tuning the distance between PMMA-domains (d_3), which impacts directly the optical properties of the MBCs. While almost colorless gels are obtained when $d_3 < 60\ nm$, blue and green colors emerge for $d_3 = 80\ nm$ and $d_3 = 140\ nm$ respectively (red is expected for even larger d_3 value as observed in Figure 2). Anecdotally, the correlation peak observed at $q = 1.85\ nm^{-1}$, originates from the distance between bottlebrush PDMS backbones, being close to 3.4 nm regardless of the HS content. WAXS is then needed to access details at lower length scales.

Beyond classical uses of WAXS, *i.e.*, identification of crystalline phases and quantification of their volume fraction, we prefer to focus here on three more original examples that we have adapted in Figure 4, from refs.[10, 20, 109].

Figure 4A, represents the WAXS (front scattering) and XRD (backscattering) 1D integrated signals measured from a PBT-PTHF MBC containing 40% in HS prepared through two common methods: hot-pressing (HP^-) and solvent casting (SC), (see also Figures 1 and 3). The idea of the authors here is to emphasize the impact of the processing route on the preferential crystallites growth direction. While XRD is performed in a "classic" way, *i.e.*, by using the X-ray "reflection" from a single film, the WAXS measurement is achieved by stacking narrow pieces of film and probing them with a X-ray beam perpendicular to the direction of stacking (see Figure 4A). Two diffraction peaks coming from the crystalline structure of PBT are of particular interest: (010) and (100), revealing the following points. i) XRD ("Front") experiments provides isotropic 2D patterns (not shown) both in HP^- and SC samples. However, while the 010 peak is stronger when hot-pressing is used, 100 dominates in solvent-cast samples. ii) In contrast, WAXS ("Side") experiments result in anisotropic 2D patterns. While the "North-South" (NS) integration makes emerge the (100) peak in hot-pressed samples, it is the (010) that dominates in the solvent-cast samples - the opposite trend is observed when considering the "West-East" (WE) direction. From these observations, the authors conclude that in spite of qualitatively similar top-views of their MBCs when using hot-pressing or solvent casting, (see Figure 1A), confronting WAXS and XRD measurements indicates that the two kinds of MBCs are quite different from a topological

point of view. Also, the apparent isotropy observed from AFM vanishes when considering the depth of the materials.

Apart from investigating static structure, WAXS is also used to highlight strain induced crystallization (SIC) upon stretching in MBCs. In Figure 4B, Zhu et al. show the impact of a cyclic tensile loading on the crystallization of the SSs in a similar PBT-PTHF MBC. Odd and even indices refer respectively to successive relaxed and loaded states. On one hand, Figure 4B*1* indicates that a higher tensile deformation promotes the crystallization of the PBT HSs, the latter remaining stable when the samples are subsequently relaxed. On the other hand, Figure 4B*2* reveals the crystallization of PTHF SSs, that however disappears when the load is removed.

Another interesting example is that proposed by Candau et al., reported in Figure 4C, where an amorphous TPU based on PEG SSs is studied. While PEG is seen to crystallize upon stretching between 200 and 300% in strain amplitude, the crystallites spontaneously melt when the material is relaxed, similarly as in the previous case. However, from 400%, PEG crystallization is surprisingly found to be permanent (compare *e.g.*, the second and the last 2D patterns in Figure 4C*1*). The authors explain this qualitative difference through the reorganization of the hard-phase into smaller domains in which HSs are aligned in the strain direction, stabilizing the SSs crystallites. They insist on the peculiar behavior of the MBCs by reminding that such a situation could not have arisen in homopolymers.

Overall, because the crystallization of SSs has a strong impact on the macroscopic mechanical properties of MBCs, this variety of behaviors appears as an excellent opportunity to tune their performances. In fact, reversible crystallization ensures a high flexibility at rest and a strong resistance under loading while permanent crystallization, possibly generated by a pre-stretching step, can provide MBCs with a much higher modulus and yield point directly from a low deformation level. This question is notably addressed in a very recent paper by Zhu et al.[121] where the authors provide a general vision of the reversible–irreversible character of SIC.

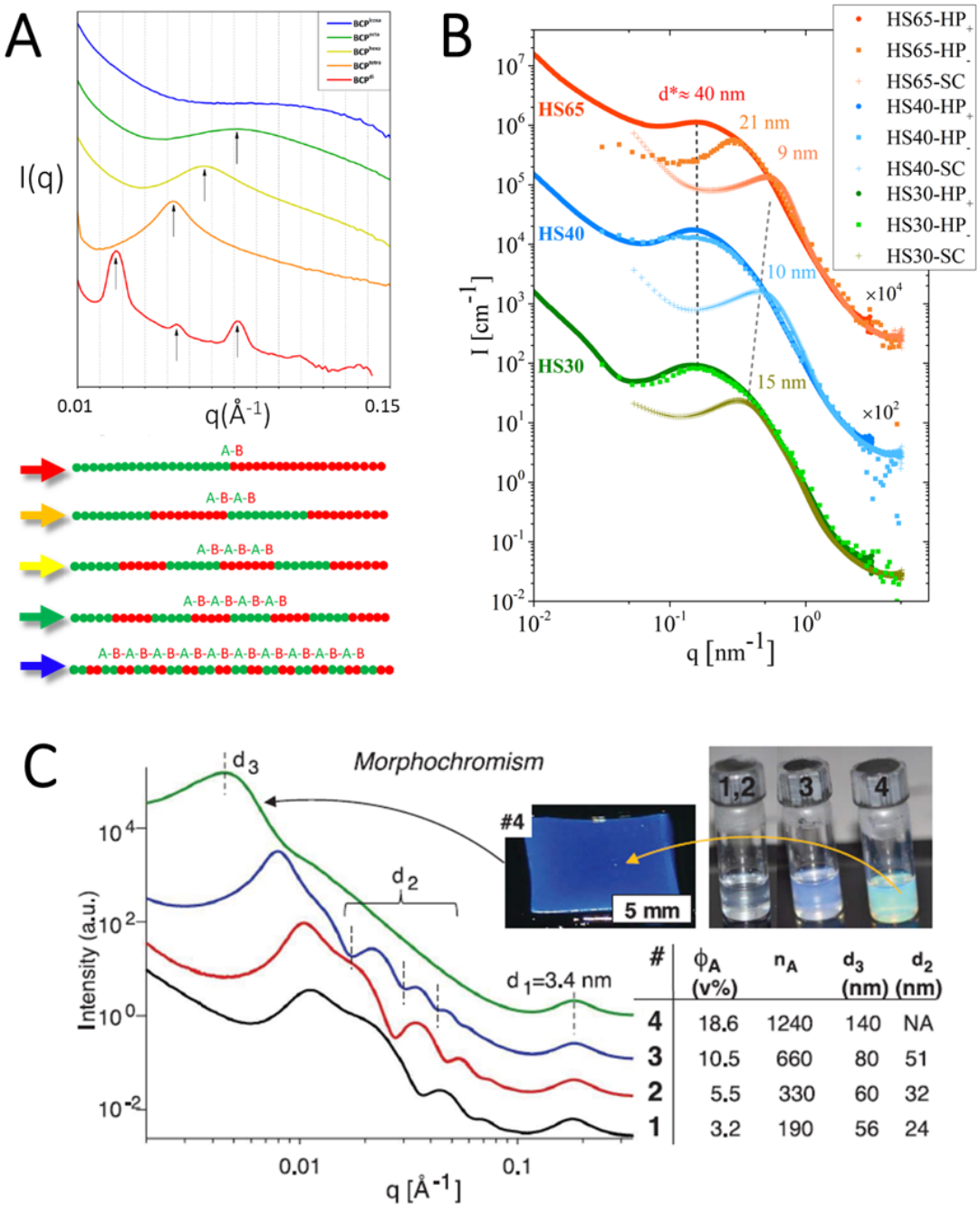

Figure 3: MBCs characterization through SAXS. A) Effect of the segmentation degree on the microstructure of a series of model MBCs made of EGMEA HSs and tBA SSs with fixed molecular weight and stoichiometry, adapted from ref.[113]. B) Effect of the processing route and HS content on commercial MBCs made of PBT HSs and PTHF SSs, adapted from ref.[109]. C) Effect of the HS length on the morphology and color of MBCs made of PMMA HSs and bottlebrush PDMS SSs, adapted from ref.[15].

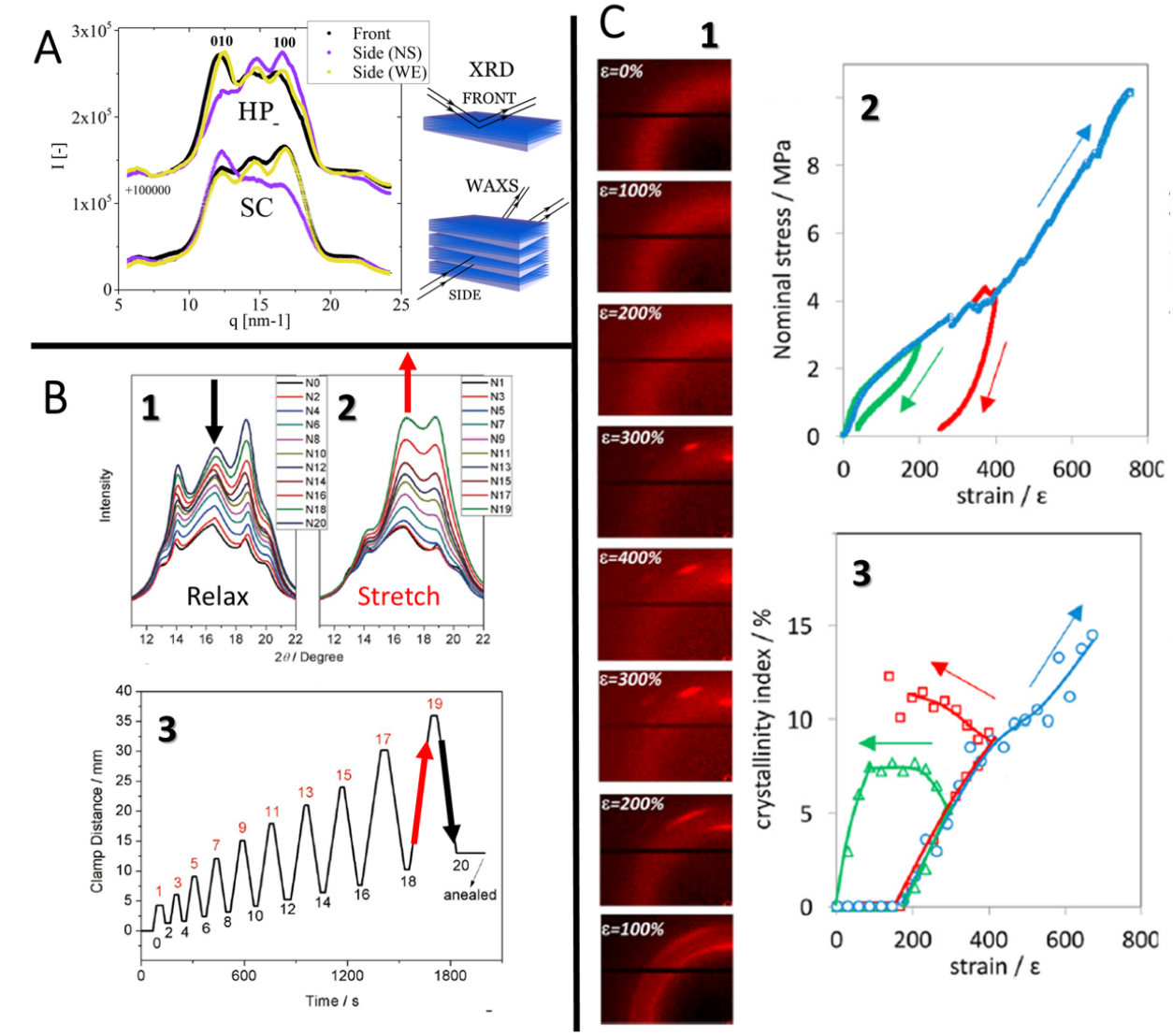

Figure 4: MBCs characterization through WAXS. A) Effect of the processing route on the crystallites' growth preferential direction in commercial MBCs made of PBT HSs and PTHF SSs, adapted from ref.[109]. B) Strain-induced crystallization of PTHF SSs upon stretching (*1.*) and their subsequent melting while unloading (*2.*). Corresponding sequential deformation (*3.*). HSs are made of PBT, adapted from ref.[20]. C) Strain-induced crystallization of PEG SSs upon stretching with crystallites remaining possibly stable while unloading. HSs are made of amorphous urethane-urea, adapted from ref.[10].

2.3 Indirect probes

This section could have been entitled: "Non-mechanical properties of MBCs". We propose here a rapid overview of the most popular techniques that provide complementary details on the multi-scale structure of MBCs, serving in section 3 to rationalize their mechanical behavior. Similarly as in the previous section, we try to emphasize "unusual" results and/or techniques with the aim to inspire the reader for his/her future work.

2.3.1 Other experimental investigations

Differential scanning calorimetry (DSC) is certainly the most popular technique to probe MBCs. In fact, it provides easily quantitative features enabling a quick and global understanding of the material's structure. Beyond the glass transition temperatures and possible melting/crystallization points of A and B species, it can be used to probe the crystallization kinetics and estimate accurately the crystalline content. Also, it may be used to detect chain relaxation in pre-constrained samples or makes emerge dynamical heterogeneities in multiphasic materials. Last but not least, the emergence of flash differential scanning calorimetry (FDSC) henceforth allows generating large amount of data in a limited time and open new experimental perspectives such as a precise investigation of cold-crystallization.[23] In Figure 5A, we present DSC thermograms (temperature ramps) measured on a PBT-PTHF MBC crystallized isothermally at 140 $°C$ for 4, 17, 25 and 70 minutes.[116] In this work the authors emphasize the bimodal character of the PBT crystallization by combining thermal and mechanical characterizations. As clearly evidenced in this figure, while the main crystallites develop immediately (at 140 $°C$) resulting in a melting peak close to $T_I = 180$ $°C$, a second "frustrated" population appears after 17 minutes of crystallization ($T_{II} = 150$ $°C$). This phenomenon is assigned to the loss of mobility of MBC chains provoked by the "primary" crystallization resulting into the creation of poorly stable hard-domains.

Figure 5B represents low-field NMR relaxometry results measured on PS-PB based diblock and star copolymers at different temperatures satisfying $T_g^{PB} < T < T_g^{PS}$.[122] These experiments, performed with a benchtop spectrometer, are known as "magic-sandwich-echo free induction decay" and provide information on the phases mobility and their relative mass

fractions. Here, the fast decay ($t < 0.02\ ms$) of the signal originates from the magnetic relaxation of the hydrogen atoms embedded into the rigid PS phase f_r whereas the quasi-plateau observed at longer time is generated by slowly relaxing protons in the mobile PB phase f_m. The clear distinction between the two contributions offers an accurate estimation of the two phases fractions evolution when changing the temperature and the polymer composition. Beyond this application, low-resolution NMR spin diffusion experiments serve notably to investigate the peculiar behavior of the interphase between rigid and mobile phases or the size of MBCs nanodomains.[123–126] Note however, that apart from the recent adaptation of these methods to benchtop spectrometers favoring their spreading in the polymer science community, spin diffusion techniques are routinely used for a relatively long time.[127].

Another popular dynamical tool to probe MBCs is broadband dielectric spectroscopy (BDS). It consists of forming a capacitor in which the dielectric part is made of the material of interest and applying an oscillatory voltage, varying its frequency from ca. 1 MHz down to 0.01 Hz. Unlike mechanical probes, the great advantage of this technique is that it provides information over 8 decades in time, allowing notably to detect local, segmental and chain relaxations in a single experiment. In Figure 5C, we present BDS results measured from a series of amorphous TPUs based on PPG SSs, varying the length of SSs and HSs while keeping the molecular weight of the MBC similar, *i.e.*, decreasing the segmentation degree from left to right. In every experiments, plotting the "conductivity-free dielectric losses" (ϵ''_D) vs. the frequency (ω) enables the detection of local glassy state motions (denoted γ and β), segmental relaxations (α_i) and an interfacial polarization contribution at low frequency/high temperature known as Maxwell-Wagner-Sillars process (in red). Of a particular interest, while a single α_{mixed} relaxation evidences unambiguously that SSs and HSs are well-mixed for high degree of segmentation, two segmental contributions appear ($\alpha_{SS-rich}$ and $\alpha_{HS-rich}$) when increasing the blocks' length indicating their phase separation. On top of this, the emergence of the normal mode (NM), arising from long PPG SSs diffusion is another proof of the growing phases incompatibility. By combining these results with DSC, SAXS and rheology experiments in two papers,[41, 128] Heydarnezhad et al. provide a deep understanding of the structure-properties of their amorphous TPUs and corresponding nanocomposites that one could be very much tempted to reproduce from other MBCs. The

task seems however more intricate for semi-crystalline MBCs because of the lack of mobility of the hard phase.

Finally, a more chemistry-oriented method to predict the phase separation of HSs and SSs has been successfully applied by Gallu et al. in TPU-bitumen mixtures. Figure 5D represents the Hansen solubility sphere diagrams of the polyol SS (left) and the MDI/BDO HS (right). In both cases, the large greenish sphere represents the zone of compatibilty of the bitumen while darker and smaller spheres stand for the SS and HS' ones respectively. The radius of each sphere is determined by performing a series of test in solvents characterized by well-known Hansen parameters.[129] Based on these diagrams, the authors clearly evidence the following points: i) the SS and the HS are not compatible, (ii) a good affinity exists between the bitumen, rich in aromatic species, and the SS, and (iii) the affinity between the HS and the bitumen is poor. By complementing their chemical analysis with SAXS experiments, the authors nevertheless demonstrate that resins present in the bitumen were likely to diffuse within the HS crystallites, provoking their swelling. Papers by Gallu et al.,[54, 114, 130] dealing with complex materials having industrial applications, well illustrate the need for both physical and chemical probes to access a global understanding of MBC based materials. In other words, they suggest that future progress in the field will necessarily pass by researchers endowed with a multidisciplinary background.

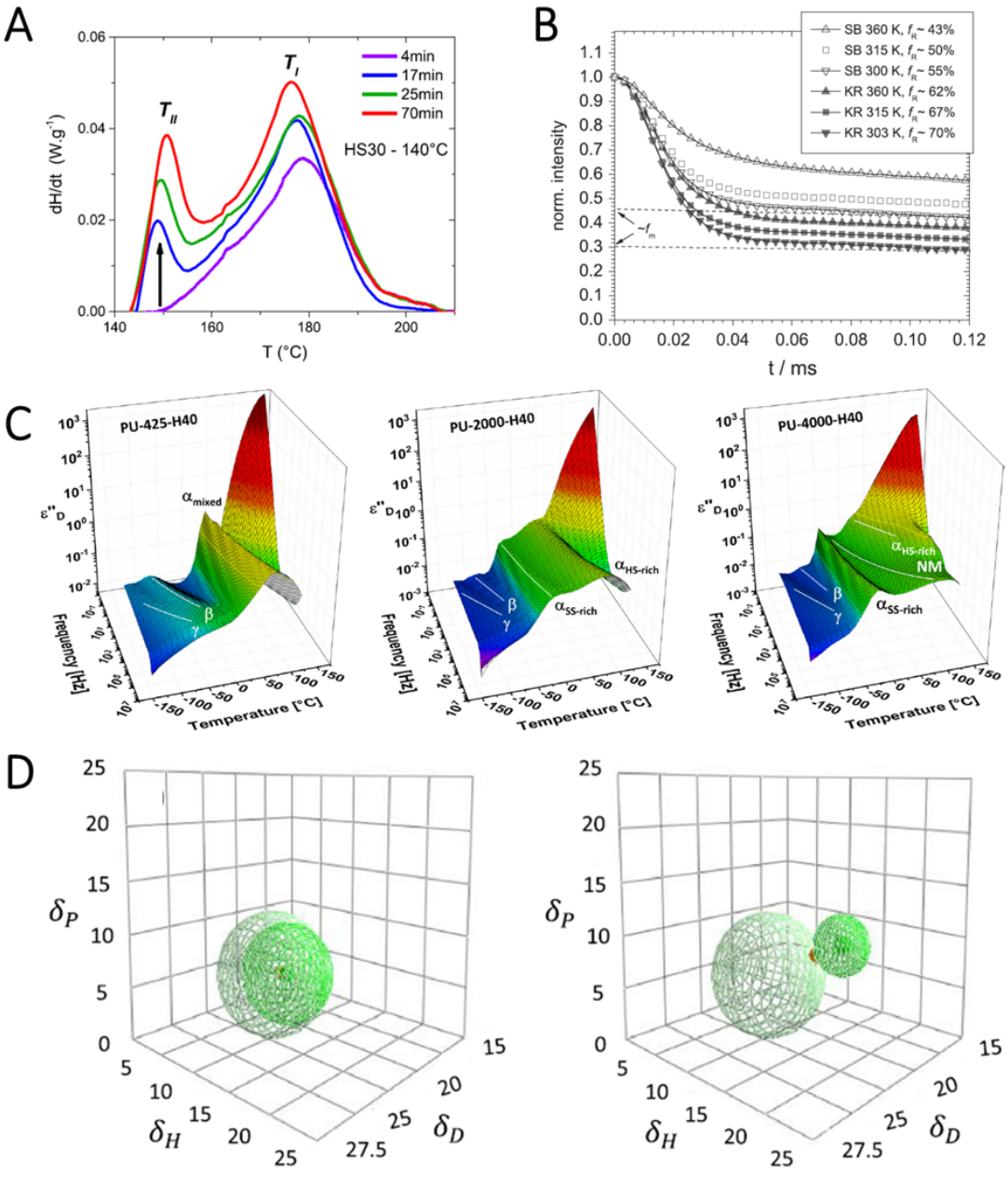

Figure 5: Non-mechanical properties of MBCs as tools to probe their structure. A) DSC evidences two crystallites population in PBT-PTHF MBCs (endo up), adapted from ref.[116]. B) Low-field NMR provides a direct estimation of soft and hard phase relative fractions in PS-PB diblock (SB) and star (KR) copolymers, adapted from ref.[122]. C) Broadband dielectric spectroscopy reveals the degree of phase separation in TPUs based on PPG SSs, adapted from [41]. D) Hansen solubility parameters sphere diagrams indicating the compatibility of a polyol SS and a MDI/BDO HS with bitumen, adapted from ref.[114].

2.3.2 Computational work

Beyond experimental investigations, the last three decades have seen the emergence of molecular dynamics simulations. Polymer science have notably taken advantage of the henceforth famous Kremer-Grest (KG) model,[84, 85] providing results well in-line with experiments and theory.[131] The general approach of the KG model (and others) consists of simulating polymer chains as a succession of beads, each of them representing a certain number of atoms/monomers according to the coarsening degree of the simulation. Overall, the interactions between two beads are modeled by a Lennard-Jones potential characterized by a distance at equilibrium (r_{eq}) and an attractive potential well (ϵ). Two successive beads in a chain however interact with each other through a finitely extensible nonlinear elastic (FENE) potential representing covalent bonds of length l_b, ensuring the "non-crossability" of the chains. An additional, but not essential, bending potential is sometimes used to tune the chain rigidity, allowing to simulate chains closer to "real" polymers.[131, 132] For every time steps, the force applied on each bead is then calculated from these potentials, providing their trajectory from Newtonian mechanics. Applying this methodology to block copolymers requires then to simulate chains of various local rigidity, being equivalent to different Kuhn lengths l_k or characteristic ratios $C_\infty = l_k/l_b$ in real polymers. Also, it requires to compute interactions for the different couples of beads, *i.e.*, AA, AB and BB resulting in a minimum of 5 different potentials to be defined. Once fixed the model parameters and the chains topology (linear,[133, 134] star,[81, 135] ring,[136, 137] ...), the simulation box is equilibrated at high temperature. One can then focus on the phase separation occurring upon cooling, by following the variation of volume (or enthalpy). The resulting structure is finally analyzed through statistical methods with the aim to quantify the phase separation[138] (and possible crystallization[134, 139, 140]) or to discriminate various segments topologies (tie, loop, dangling). The latter analysis is of great interest to rationalize the mechanical behavior of polymers,[141, 142] notably through the determination of the molecular weight between entanglements.[143] Because molecular dynamics simulations provide a topological resolution of the chains together with the possibility to investigate prospectively non-synthesized molecules, they appear as an unavoidable tool in the coming years. As men-

tioned in introduction, they have recently allowed to partly solve one of the most challenging question in polymer physics concerning the relation between the molecular sequence and the microstructure of proteins.[76] Their future spreading and systematic utilization will however be conditioned by the progress of computer capabilities. In fact, apart from using large processor clusters, molecular dynamics simulations are typically restricted to a lengthscale corresponding to a few tens of nanometers, being insufficient to unravel macroscopic properties. "Lighter" computational methods such as SCFT-oriented simulations evoked in section 2.1 appear therefore in this context as a great alternative. In Figure 6, we have adapted recent results from refs.[81, 134, 137] focusing on the link between the molecular topology and the resulting microphase separation for linear MBCs, star MBCs with diblock arms, and diblock ring polymers respectively.

Figure 6A*1-2* presents enthalpy variations of pentablock and triblock systems of various SS content upon cooling. The HS length is fixed in all the simulations. The chain size is independent of the SS content but it is larger for pentablocks than for triblocks. The model parameters are adjusted so that SSs and HSs resemble to PTHF and PBT moieties relatively. Beyond the expected fall of the crystallization enthalpy when increasing the SS content in both types of chains, the crystallization temperature of pentablocks is observed to decrease whereas it remains almost constant in triblocks (see arrows indicating the exothermic peaks position at the bottom of each figure). This result suggests strongly that the phase separation is anterior to the crystallization in triblocks, *i.e.*, that HSs have already formed large enough domains so that their crystallization temperature does not depend on their size anymore. The opposite trend observed in pentablocks indicates, conversely, that HSs crystallization is the driving force inducing the phase separation resulting notably in a refinement of the crystalline structure, *i.e.*, a higher number of crystallites and a reduction of their size. As mentioned above, a great asset of these simulations is that physical interpretations can be directly confronted to structural features. In fact, plotting the HS beads pair correlation function g in Figure 6A*3* confirms the above scenario. While g remains almost flat from a temperature T=3 down to T=2 in pentablock copolymers, it indicates much stronger correlations in triblocks, synonymous of a more advanced phase separation prior to the crystallization (occuring from T=2 for neat HSs). Based on these results, the authors then

propose to analyze quantitatively the topology of the SSs with the aim to bridge the molecular architecture and the MBCs' microstructure.[134]

Another example of recent computational work is that of star block copolymers as studied by Spencer and Matsen through an original SCFT approach.[81] The latter requires a much shorter calculation time than molecular dynamics simulations as it does not consider beads nor time, allowing to model larger systems. Here, the authors consider star polymers in which arms are made of diblock copolymers resulting in various morphologies according to the temperature and the relative fractions of A and B blocks (spherical, cylindrical, lamellar or disordered). In Figure 6B*1-3*, we adapted their results illustrating possible star conformations for a cylindrical microphase separation (obtained for 25% of red blocks - 2D representation). The authors pay a particular attention to the ability of star polymers to bridge distinct red domains as a function of the total number of arms M, and among them, the ones connected to the "first cell" m appearing in green. In Figure 6B*4*, their analysis emphasizes that the most probable conformation as well as the position of the star's center evolve with increasing the number of arms. In particular, the configuration presented in Figure 6B*2*, *i.e.*, $m = 4$ seems to be the most probable when M is fixed to 9, implying the displacement of the star center to a position being equidistant from three red spheres, leading to a maximum of bridging degree. In their conclusion, the authors remind that although the morphology of the phase separation, *i.e.*, lamellar, cylindrical or spherical, strongly increases the fraction of bridging molecules (in this order), switching from a linear to a star architecture can have a similar impact, explaining the improved mechanical properties observed experimentally in refs.[144, 145].

A last illustration of the structural richness of block copolymers beyond the usual linear diblock chains is that of amphiphilic "*Janus*" ring polymers proposed by Jehser and Likos.[137] Although the authors do not deal, strictly speaking, with MBCs in this case, we believe that their work is worth to highlight since it focuses on a recently developed polymer topology, mostly restricted to homopolymers so far.[146–148] The investigation concerns the self-assembly of *Janus* rings in solution varying the relative fractions of A and B species, the ring flexibility, the solution concentration and the temperature. In Figure 6C*1*, we report the coarse-grained generic structure of the molecules while Figures 6C*2-3* represent respec-

tively solutions of semi-flexible diblock rings containing f_A =20% and 50% of attractive (red) beads. Note that the concentration in beads is identical in both cases and that the temperature is similar. Interestingly, simulations reveal that the aggregates' morphology is spherical ($f_A = 12\%$) before to become growingly toroidal ($20\% < f_A < 40\%$). However, at larger degree of amphiphilicity, $f_A = 50\%$, the torus is not the most favorable conformation anymore, and is replaced by a mixture of spherical, toroidal and prolate aggregates. These unique network structures, not accessible with other molecular architectures, may represent new opportunities to design materials of unprecedented properties, notably by mixing them with linear and/or star (co)polymers of similar chemical nature, as already imagined by Hou et al. for homopolymer rings.[147]

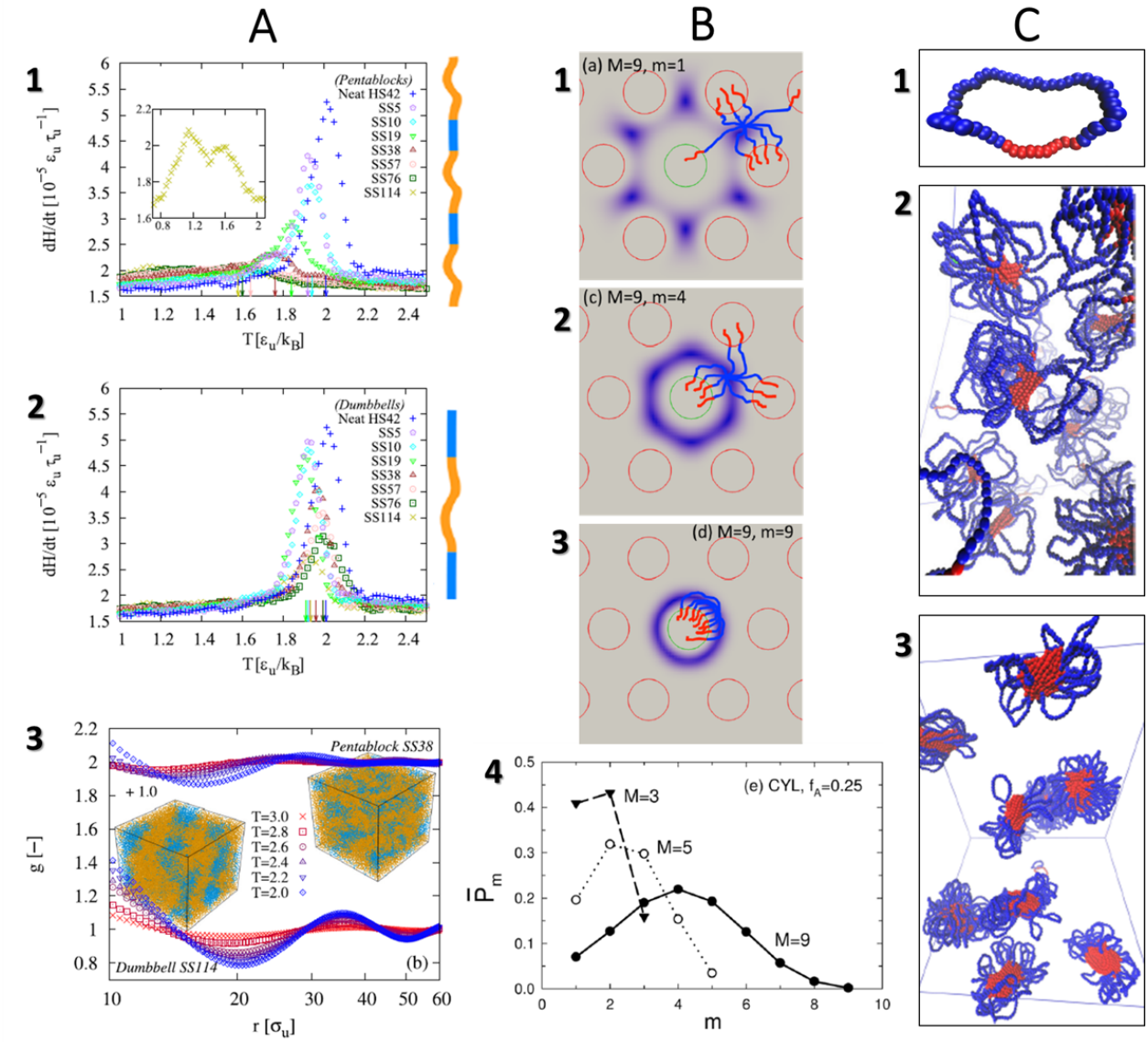

Figure 6: Computationnal investigations of block copolymers of various topologies. A) Enthalpy variation upon cooling for *1.*pentablock and *2.*triblock ("dumbbell") linear copolymers. *3.* Corresponding evolution of the pair correlation function and visual representations of two selected copolymers, adapted from ref.[134]. B) Conformation analysis of a star copolymer embedded in a hexagonal biphasic structure. *1-3.* Visual representations emphasizing domains bridging. *4.* Probability of finding a star as a function of m for M=3, 5 and 9, adapted from ref.[81]. C) Solution of diblock ring copolymers. *1.* Single molecule. *2-3.* Assembly of rings containing respectively 20% and 50% of (red) attractive units, adapted from ref.[137].

3 Towards the rationalization of mechanical properties

3.1 Elements of theory: on the elastic modulus of polymer networks

The present section provides a framework concerning the relationship between the microstructure of a polymer-based system and its elastic modulus. The general concepts that are recalled here will serve as a basis for section 3.2 where recent ideas connecting the topology of MBCs with their mechanical properties will be presented.

Entangled networks

The simplest model that captures rubber elasticity is the "affine model". It assumes that a rubber-like material can be seen as a network made of connected strands, and that applying a macroscopic deformation on the material results on the same deformation in each strand. The latter can then be used to calculate the variation of entropy in a strand, which depends on the distance between its two ends, and further extended to the whole network. Then, by ignoring any change in enthalpy, the free energy of the whole network can be simply expressed as the product of the temperature and the corresponding entropy variation. Following this track leads to the well-known expression of the shear modulus[149]

$$G_0 = \nu k_B T = \frac{\rho R T}{M_s} \tag{7}$$

where ν is the number density of strands, ρ is the mass density of the network, R is the perfect gas constant and M_s is the average molar mass of a strand. This equation states that the modulus of a polymer network is $k_B T$ per strand, regardless of its chemical nature. Based on the same philosophy, more advanced models have been developed such as the "phantom model" that incorporates chain ends fluctuations leading to a lower estimation of the shear modulus. Practically, Equation 7 is however mostly used for its simplicity and connects in a straightforward way the shear modulus and the apparent molar mass of the strands. In the case of an amorphous polymer network made of entangled chains, the "tube model" originally developed by Doi and Edwards,[150] makes use of M_e, *i.e.*, the molar

mass between entanglements. This parameter varies from ca. 1 to 50 $kg\ mol^{-1}$ for most of common polymers[151] and its corresponding dimension called the "tube diameter", denoted R_e hereafter, is typically of a few nanometers. It can be calculated from the polymer Kuhn length b such as

$$R_e = bN_e^{0.5} = b\left(\frac{M_e}{M_0}\right)^{0.5} \tag{8}$$

where N_e is the number of "Kuhn-mer" of molar mass M_0 per entangled strand.

Supramolecular entangled networks

Beyond purely entangled networks, one can then consider the more complex case of supramolecular polymers, endowed with chemical moieties acting as stickers between the chains. The most popular model rationalizing the linear mechanics of entangled supramolecular polymers, is known as the "sticky-reptation model". It was proposed in 1991 by Leibler, Colby and Rubinstein[72] where a new version of Equation 7 was reported as follows

$$G_0 = \rho RT\left(\frac{1}{M_e} + \frac{p}{M_{stick}}\right) \tag{9}$$

where p is the probability of the stickers to be active and M_{stick} is the molar mass between stickers, both parameters accounting for the network's stiffening that originates from the presence of additional topological links. In this model, active stickers are seen as tetrafunctional nodes with no excluded volume.

Nanocomposites

The rationalization of the mechanical properties becomes more intricate when considering multiphasic rubbers. A common situation is that of nanocomposites consisting of dispersing spherical hard particles into the rubber background. For low volume fraction of fillers, the hydrodynamic theory of Einstein[152] and Smallwood[153] was adapted successfully to rubbers by Guth[154] allowing to describe the reinforcement χ as

$$\chi = \frac{G}{G_0} = 1 + 2.5\Phi + 14.1\Phi^2 \tag{10}$$

where Φ is the volume fraction of fillers and G is the modulus of the composite. Note that other values of the quadratic term prefactor were also reported, see *e.g.*, ref.[155]. Considering then the case of anisotropic fillers results in a new version of Equation 10, accounting for the aspect ratio of the fillers r_a such as

$$\chi = 1 + 0.67 r_a \Phi + 1.62 r_a^2 \Phi^2. \tag{11}$$

In absence of strong interactions between the polymer phase and the reinforcing fillers, Equation 10 and 11 are usually found to predict satisfyingly the modulus of composites loaded with less than 10 *vol.*% in particles. However, increasing the loading above this threshold requires to think beyond hydrodynamics.[156] In particular, the percolation of fillers is often evoked to rationalize the strong upturn of the reinforcement observed above $\Phi = 10$ *vol.*%. In this context, the most common picture is that of the emergence of an immobilized polymer layer bridging neighbor particles, resulting in a sudden hardening of the material at low deformation[157, 158] and participating to the reduction of the linear regime amplitude, known as the "Payne effect".[159] However, because of the variety of fillers, processing techniques and interactions with the host polymer, no model allowing a systematic and quantitative prediction has truly emerged.

Semi-crystalline homopolymers

Another example of multiphasic polymer network is that of semi-crystalline homopolymers, where the multiscale structure and the network topology are hardly quantifiable. In this case, phenomenological models, based on usual rules of mixtures inspired by (macro)composites materials, are often used to rationalize the elastic modulus. They consist mainly of parallel, series or mixed arrangements of soft and hard phases, resulting respectively in the two former cases in

$$\chi = \frac{\Phi E_c + (1 - \Phi) E_0}{E_0} \tag{12}$$

and

$$\chi = \frac{E_c}{(1-\Phi)E_c + \Phi E_0} \tag{13}$$

where E_c and E_0 stand for the longitudinal elastic moduli of the crystalline and amorphous phases respectively. More advanced models, relying on arbitrary parameters quantifying the degree of series or parallel association between the two phases have been developed until recently[160, 161] without however making convincingly the link between the polymer conformation, the phase separation and the mechanical properties.

Other attempts based on topological considerations can be found in the literature.[162] They rely on the fact that mechanical properties of semi-crystalline polymers, notably their stiffness, originates from the amorphous chains segments connecting crystallites. The latter are alternatively identified as "tie molecules", *i.e.*, chain segments connecting covalently two different crystallites, or "loops", *i.e.*, pairs of chains segments being entangled with each other forming a topological nodes between crystallites. A noteworthy example, based on a modification of the rubber elasticity theory, is the model proposed by Krigbaum et al.[163] accounting for the non-Gaussian conformation of tie molecules expressed as

$$G = \nu k_B T \times \mathcal{F}(\Phi, N_e) \tag{14}$$

where $\mathcal{F}(\Phi, N_e)$ is a function describing the strain in the amorphous phase and the non-Gaussian conformation of the tie chains. It depends on both the crystallites content Φ and the length of the elastically active chains N_e that controls the probability of occurrence of tie molecules (lower probability for higher N_e).

Multiblock copolymers

Although the growth of the elastic modulus as a function of the hard segment content has been extensively studied in the MBCs literature, its theoretical rationalization still remains elusive. This lack of modeling probably comes from the variety of parameters to be considered, impacting both the microphase separation and the chains conformations. Experimentally, an exponential trend seems to emerge when plotting the reinforcement as a function of the hard-phase volume fraction. This was tentatively rationalized through an empirical model (still based on E_c and E_0), by Wegner et al.,[164] then Gaymans et al.[82], indicating

$$\chi = \left(\frac{E_c}{E_0}\right)^{\Phi}. \tag{15}$$

This trend was qualitatively confirmed by Nébouy et al.[165] who recently found $\chi = e^{A\Phi}$, with $A \approx 18$, on a wide variety of MBCs. However, the fact that A must be much greater than $ln\left(\frac{E_c}{E_0}\right)$ clearly indicates that considering the intrinsic modulus of the hard-phase, probably close to a few GPa, is not relevant to describe the macroscopic modulus of MBCs. In other words, E_c simply cannot be e^{18} times higher than E_0.

3.2 Mechanical behavior in the solid state

3.2.1 Elastic modulous of MBCs

The main challenge of rationalizing the elastic modulus of phase-separated MBCs resides in the contemporaneous consideration of microphase separation and molecular topology. In fact, similarly as semi-crystalline polymers, MBCs are made of different phases that are connected covalently. As indicated in the previous section, this peculiar morphology was alternatively modeled by using two philosophies based on (i) rubber elasticity, *i.e.*, a molecular picture, or (ii) hydrodynamics, *i.e.*, a composite-oriented vision. While the former is well adapted to describe the mechanics of a monophasic amorphous polymer network and the latter well captures the impact of additional fillers, none of these concepts, taken separately, seems however satisfactory to rationalize the complexity of solid MBCs.

As illustrated in Figure 7A (adapted from ref.[54]), the phenomenology is clear: increasing the fraction of HS within the copolymer chain results in a higher content in hard-phase, measurable through DSC, that one can invoke to explain qualitatively the enhancement of the rubbery modulus, as done in many papers.[22, 26, 27, 30, 116, 166–170] Also, for a given fraction of hard-phase, one can legitimately wonder what is the impact of the hard-domains size on the elastic modulus. This effect is illustrated in Figure 7B, adapted from ref.[171] where we report that increasing the width of PBT ribbon-like crystallites in a PTHF background (by changing the processing conditions), enhances the reinforcement for a given Φ. Note that this may not be expected from the reader who is trained in nanocomposites science because it indicates that the elastic modulus diminishes when increasing the specific

surface of the reinforcing phase. This further demonstrates the necessity to bring topological considerations into the debate.

The quantification of both these phenomena has been recently addressed by us on the restricted case of well-defined MBCs based on short T4T HSs and PTHF SSs.[166] Our approach is illustrated in Figure 7C where the molecular picture of the neat PTHF (*1.*) and the corresponding MBC (*2.*) containing ribbon-like crystallites are represented. In this work, the main idea consists of considering crystallized HSs as additional topological links, acting in cooperation with chain entanglements. For a sphere of volume V_e corresponding to the tube diameter R_e, we hypothesize that the number of topological links passes from 1 (entanglement per chain) to N_{ce} ($>> 1$, see Figure 7C). This latter parameter represents the number of crystallized HSs determined from the intersection of the crystalline ribbon and the sphere of volume V_e as illustrated in Figure 7C*2*. It evaluates somehow the degree of connectivity of the network close to a crystallite that acts as a "macro" topological node. For crystalline content lower than 10 *vol.*%, we provide the following equation that describes the reinforcement as a function of the volume fraction in crystallites Φ and the ribbons' width W

$$\chi = 1 + \Phi(N_{ce} - 1) = 1 + \frac{R_e d^{*2}}{nR^2 H}\Phi^2 = 1 + \frac{R_e}{R^2}W\Phi. \tag{16}$$

Here, d^* is the average distance between ribbons, H is the length of the HS, corresponding to the ribbons' thickness, n is a structural parameter being either 1 or 3 depending on the ribbons arrangement and R is the crystalline cell parameter, assumed to be identical in both transverse directions of the chain axis. Note that once identified R_e from rheology (see Equation 7) and the average section of the crystallite W from SAXS, the determination of N_{ce} is straightforward (see Figure 7): $N_{ce} = N_w\ N_{Le} = \frac{W}{R}\ \frac{R_e}{R}$.

Based on this model, which provides a quadratic dependence of the MBC modulus as a function of Φ – similarly as hydrodynamics models presented in section 3.1 but with a much larger prefactor – and its extension to $\Phi > 10$ *vol.*% developed in the same article, we obtained a global reinforcement law such as $\chi = e^{A\Phi}$, with $A \approx 18$. Later, we compared this trend to a dozen of papers dealing with various MBCs of growing HSs content. This comparison is reported in Figure 7D where *1.* is a lin-lin plot and *2.* is a semi-logarithmic

representation, adapted from ref.[171], suggesting a possible universal trend. Although some results significantly deviate from the solid black line that represents our prediction, most of these points are related to MBCs presenting peculiar morphologies, being quite different from usual TPEs. For example, circled data refer to diblock copolymers or to MBCs made of unentangled SSs, not satisfying the hypotheses of our model.

While the topological approach (Equation 16) seems therefore well adapted to rationalize the reinforcement at low and moderate hard-phase content, a major challenge concerns the understanding of the behavior at higher Φ. In this regime, simple geometrical considerations regarding the Gaussian statistics of SSs and the distance between hard domains indicate that the soft background must be out of equilibrium, impacting necessarily the reinforcement. The quantification of the SSs dynamical slow-down, reminiscent of the immobilized polymer layer reported in attractive nanocomposites,[172, 173] appears therefore to be a key factor to rationalize MBCs hardening. In this context, ongoing molecular dynamics simulations performed in our group suggest that the reinforcement upturn observed at high Φ originates from sluggish-SSs bridged hard-domains rather than from a continuous HS-crystalline phase spanning the whole MBC structure. An example is provided in Figure 7E, where *1.* and *2.* represent the situation at $\Phi = 4$ *vol.*% and 16 *vol.*%, respectively. Blue segments stand for the crystallized HSs while orange ones represent slow-down SSs located close to the interface, showing the presence of a hybrid (HSs+sluggish SSs) percolated network. Unperturbed SSs, fulfilling the rest of the simulation box, are not shown for clarity. The discrimination between the various types of SS is achieved by following the time dependence of the mean-square displacement of each simulation bead.

Lastly, we want to point that although this approach has only been used on crystallizable MBCs so far, it would simply require to determine the size of amorphous hard domains and estimate the corresponding number of HS to extend it to a wider range of MBCs, notably amorphous TPUs.

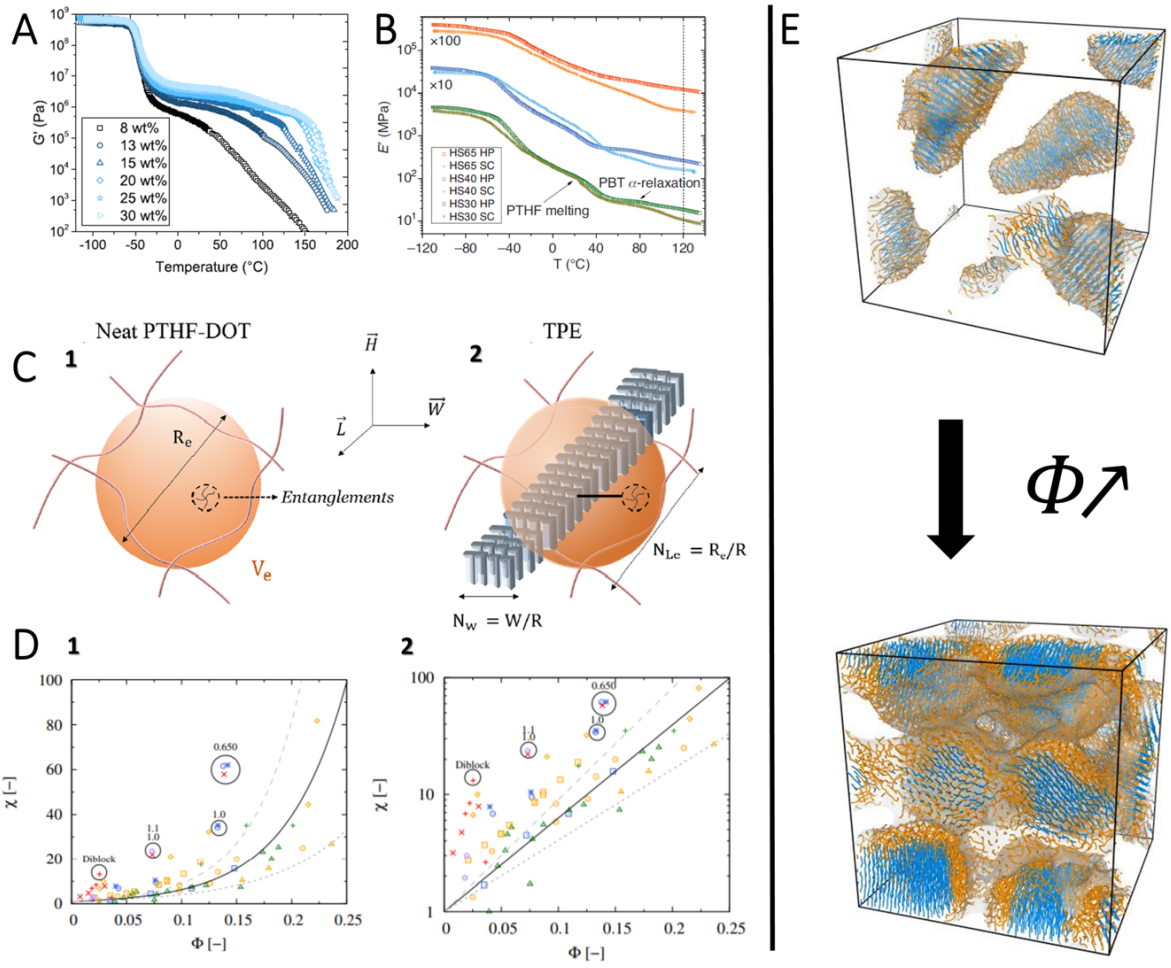

Figure 7: Reinforcement in MBCs. A) Dynamic temperature sweeps on TPUs of growing content in HSs, adapted from ref.[54]. B) Analogous measurement on PBT-PTHF MBCs varying both the content in HS (from green to red) and the processing route (various shades). Data were shifted for clarity, adapted from ref.[171]. C) Schematic representation of a topological approach used to rationalize the reinforcement. The comparison is made between *1.* a neat amorphous polymer and *2.* a thermoplastic elastomer, adapted from ref.[166]. D) Reinforcement as a function of Φ in semi-crystalline MBCs of various chemical natures. *1.* and *2.* are linear and semi-log representations respectively, adapted from ref.[171]. E) Molecular dynamics simulations highlighting the percolation of a hybrid network responsible for the reinforcement upturn at high Φ, courtesy of J. Morthomas (INSA-Lyon).

3.2.2 Non-linear properties: focus on tensile tests

Beyond their mechanical properties at low deformation, bulk MBCs are widely investigated from their moderately non-linear regime up to their failure point. Because of its simplicity, the most popular method is the uniaxial tensile experiment consisting of stretching a rectangular piece of material in a given direction at a constant speed, or constant Hencky strain rate ($\dot{\epsilon}$) when possible, with the aim to relate the macroscopic stress to micro-structural features. At the lowest deformation, typically below 20%, MBCs behave as quasi-elastic materials, *i.e.*, their deformation is reversible and the hysteresis loop is almost non-existent (loading and unloading steps show a similar profile). In this regime, the elastic modulus can be rationalized from the MBC structure at rest (see previous section). Increasing further the strain results in the apparition of a yield point, *i.e.*, a sudden fall of the apparent modulus, indicating the occurrence of non-reversible events such as chains pull-outs from hard-domains. Above this threshold, MBCs usually present a strain hardening regime that is explained by the alignment then stretching of the elastically active SSs (tie molecules and entangled loops) bridging the hard-domains, which progressively fragment. Generally, this effect keeps on growing until the catastrophic failure of the material at the very last stage of the experiment. Although this global picture has been well-established in MBCs and semi-crystalline homopolymers for decades thanks to *in-situ* experiments probing conjointly mechanical behavior and structural evolution, its accurate quantification based on a molecular/topological approach is not fully understood.

We report in Figure 8, recent tensile tests and schematic structural evolutions summarizing the effects of the molecular architecture, the strain induced crystallization, the temperature and the strain rate on the mechanical behavior of MBCs under large strain amplitude.

Figure 8A, adapted from ref.[174], well summarizes the evolution of tensile properties with changing the architecture of linear MBCs. As expected, increasing the PBT HS content in short PBT-PTHF copolymers (*1.*) results in their progressive stiffening over the whole strain range, caused by the presence of larger hard-domains evidenced through a higher melting point in DSC. However, their strain at failure remains overall unchanged and quite

low because of the lack of entanglements (the three copolymers satisfy $M < 15\ kg\ mol^{-1}$). More interestingly (*1. vs. 2.*), increasing the chains length up to $25 < M < 45\ kg\ mol^{-1}$, makes clearly emerge the role of bridging segments. The strain at failure passes from ca. 16% in short MBCs up to 150-600% in longer ones, indicating a much higher degree of connectivity between the hard-domains, provided by entangled SS loops and tie molecules. This observation is logically accompanied by a pronounced strain-hardening synonymous of a significant stretching of the SSs prior to the MBCs failure. In this case (*2.*), a higher content in HS is seen to promote the strain hardening while diminishing significantly the strain at failure because it is achieved through a reduced number of longer HS in the chains. This suggests therefore a coarsening of the microstructure, resulting finally in a raise of the strength and fragility.

Another promising characteristic of certain MBCs is their ability to crystallize upon stretching (see also Figure 4). An example is reported in Figure 8B, adapted from the work of Candau et al.[10] on PEG SSs based TPUs. Herein, the authors show convincingly that SIC, which results in stable SS-based crystallites, can be used to tune the mechanical properties of MBCs at any strain amplitude. While the unstretched material is characterized by a large strain at failure and a limited corresponding stress, its pre-stretched version shows quite different features. First, the partial crystallization of PEG results in a higher fraction of hard-domains leading to a strong reinforcement at low strain amplitude. Then, the presence of further hard-domains, which originate from both the fragmentation of pre-exisiting HS lamellae and the apparition of new SS-based crystallites, dramatically shorten the flexible SS average length resulting in a quicker stress divergence and a much higher stress at failure.

A less commonly investigated variable in solid MBCs is the temperature. In Figure 8C, we adapted the work of Aime et al.[175] showing yet, its dramatic impact on PBT-PTHF (or PEG) MBCs tensile properties. In their article, the authors manage to predict accurately the strain at failure of their PTHF-based MBC by modeling the kinetics of formation and breakage of physical bonds between HSs through the Eyring's rate equation

$$k(\sigma, T) = k_0\ exp\left(\frac{\Delta G}{k_B T}\right) sinh\left(\frac{\sigma v^*}{k_B T}\right). \tag{17}$$

Here, k describes the evolution of the amount of associated HSs, k_0 is a reference rate, ΔG is

the activation energy of bond breaking, v^* is the activation volume and σ is the stress that depends on the fraction of associated HSs in the MBC assuming to vary from 100% down to a low-treshold corresponding to the percolation of the stress bearing network. In other words, and because entanglements are not considered in this model, this threshold represents the limit at which the material's failure happens. By using this formalism, Aime et al. provide a complete picture of their MBC failure, which rationalizes in an elegant way the impact of the temperature, chain length, and interactions between HS. Nevertheless, they admit that further development considering the morphological changes such as the lamellar to fibrilar structures transition and the chain alignment, as well as considering the entanglements as additional topological obstacles, should further be implemented in future works.

Some of these aspects, notably concerning the role of the entanglements, have been considered by the same group in a more recent work dealing with well-defined PBT-PTHF MBCs.[88] In this paper, the authors explain the role of the molecular weight, the temperature and the strain rate through a new "mechanistic" model that describes the network from the molecular length scale. We adapted this work in Figure 8D-F showing respectively: (8D) tensile experiments data measured from two MBCs (M = 29 and 50 $kg\ mol^{-1}$) at either $\dot{\epsilon}$ = 0.17 s^{-1} or 0.0017 s^{-1} at room temperature, (8E) a schematic representation of the microstructure upon stretching and (8F) a cartoon that emphasizes the various molecular mechanisms captured by the model. The latter relies on counting the number of stress bearing units (denoted SBU) in the system at each stage of the deformation, without including the crystallites morphology. Similarly as in their previous work, the authors assume that once a couple of HSs is separated, it cannot reform, and that the temperature does not allow any SIC, which is evidenced in some of their experiments. The main equation of the model is the following :

$$SBU(f) = [1 - f_{dang}(f)] \left(\frac{\rho}{M_e}\right) + (1 - f) \langle N_{cryst} \rangle \left(\frac{\rho}{M}\right) \tag{18}$$

where the variable f is the fraction of HSs pulled out from the crystallites during deformation, $\langle N_{cryst} \rangle$ is the average number of HSs belonging to the crystal phase at rest and f_{dang} is the weight fraction of dangling end in a chain (considering both associated HSs and entanglements as topological nodes). In this equation, the first term represents the contri-

bution of the entanglements (of molar mass M_e), characterized by a relaxation time τ_e that only depends on the temperature. This parameter is then used to calculate the relaxation time of the dangling ends (τ_{dang}) being crucial to determine whether they act as SBU or not. Simply, a dangling end is considered as elastically active for $\tau_{dang} > 1/\dot{\epsilon}$. On the other hand, the second term is directly related to the non-relaxing chain segments located between two associated HSs. As illustrated in the previous section for the prediction of the elastic modulus at rest, we believe that this kind of approach, relying on the network topology, is promising to rationalize the structure-properties relationship of MBCs. However, a global model, considering the whole set of morphological changes, as well as their dependence on temperature and strain rate has not been provided yet. It seems nevertheless to be required prior to apprehend the more complex case of semi-crystalline homopolymers.

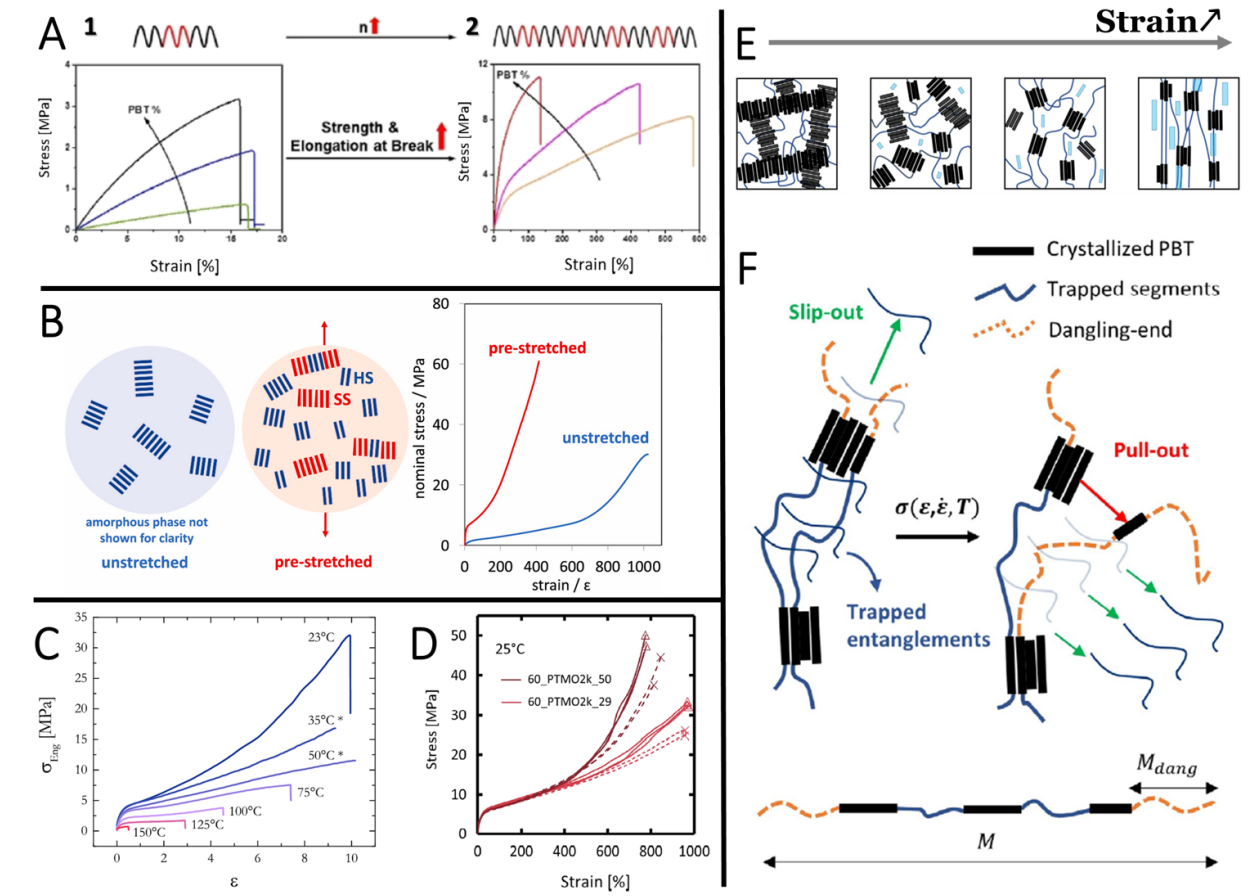

Figure 8: Uniaxial tensile tests performed on MBCs. A) Effect of *1.* PBT content and *2.* number of segments on the large deformation behavior of PBT-PTHF MBCs, adapted from ref.[174]. B) Schematic representation of the strain induced PEO SSs crystallization and its impact on the stress-strain curve of corresponding TPUs, adapted from ref.[10]. C) Effect of the temperature on the stress-strain curves of PBT-PTHF MBCs, adapted from ref.[175]. D) Effect of the chain length (red and brown refer respectively to 50 and 29 $kg\ mol^{-1}$) and strain rate (solid and dashed lines refer respectively to 0.17 and 0.0017 s^{-1}) on the stress-strain curves of PBT-PTHF MBCs, adapted from ref.[88]. E) Schematic representation of the corresponding MBC morphology upon increasing the strain. F) Schematic representation of the phenomenology rationalizing the stress-strain curves in corresponding MBCs. (E and F are adapted from ref.[88] too.)

3.3 Mechanical properties of multiblock copolymer melts

3.3.1 Linear rheology

Because MBCs are thermoreversible materials that offer the possibility to be handled from the melt state, rheology techniques have been extensively used to probe and modify (next section) their structural features. A frequent approach consists of comparing the response of melt MBCs with the "ideal" behavior of homopolymers, satisfying, *e.g.*, the Maxwell model or the time-temperature superposition (tTS) principle. In Figure 9, we have gathered works on various block copolymers that particularly highlight these deviations. A canonical example is presented in Figure 9A, adapted from a paper published in 1999 by Kossuth, Morse and Bates, where a schematic representation of the storage modulus is given for different morphologies of diblock copolymers.[176] While the usual plateau modulus G_N, which originates from the chains entanglements, is insensitive to the higher length scale structure, the usual flow regime related to chain diffusion observed at lower frequency, is strongly impacted by the phases morphologies. Here, the reference state corresponding to a homogeneous polymer is named "disordered" and satisfies the classic picture $G' \sim \omega^2$. By increasing then the degree of symmetry of the attractive phase, *i.e.*, passing from a lamellar to a cylindrical and finally to a cubic lattice, the exponent of the storage modulus power law progressively decreases down to 0. By using SAXS in the latter case, the authors report that the corresponding plateau modulus G^0_{cubic} scales with the distance between microphase separated domains d^* such as $G^0_{cubic} \sim d^{*-3}$, being in line with the general entropic elasticity theory despite its great sensitivity to the strain amplitude. Although this work focuses on model di- and triblock copolymers only, it provides a comprehensive framework to apprehend the linear viscoelastic behavior of MBCs.

In Figure 9B, we report a temperature sweep loop performed on an olefin MBC, adapted from ref.[177]. This kind of test is commonly used to characterize phase transitions, particularly to detect crystallization and melting points in semi-crystalline MBCs. This experiment nicely evidences the thermoreversible character of the MBC by showing a highly reproducible storage modulus in both melt and crystalline states, regardless of the direction of the temperature gradient. It also shows the typical supercooled domain, *i.e.*, different temperatures

of transition when cooling or heating due to kinetics effect. From this point of view, the MBC cannot be distinguished from a semi-crystalline homopolymer.

The distinction appears when considering isothermal characterizations in the melt state such as the tentative master curves presented in Figure 9C, adapted from the same article. In this case, horizontally shifted frequency sweeps are completed by inverted creep measurements that provide data over three additional decades in time and demonstrate the thermal stability of the material. Here, it appears that high frequency data (storage modulus) well collapse on the same master curve indicating that the polymer is self-similar at short time, similarly as in Figure 9A or in homopolymers. (Note that higher frequencies cannot be reached because of rheometry technical reasons and that further cooling would provoke crystallization). However, focusing on the low-frequency regime clearly evidences that the material is not fully homogeneous, including ca. 100 °C above its melting point. These apparent 3-segments broken lines are referred as "disordered with fluctuations" in the above-mentioned Kossuth's article, indicating the presence of a slight but indelible phase separation. In spite of their visible thermally activated nature, these residual interactions are characterized by a "clock" sufficiently different from the one corresponding to the monomer friction to prevent the successful application of the tTS principle.

In Figure 9D, adapted from ref.[178], the situation is even clearer. While a frequency sweep test measured on PBT-PTHF MBC melt shows a quasi-Maxwellian behavior with $G' < G''$ at relatively high frequencies, its consistent extension towards lower frequencies by means of a creep measurement reveals the presence of a true secondary plateau close to 100 Pa. In addition, the continuous fall of G'' in the corresponding window confirms the appearance of a true elastic network, characterized by an apparent cell parameter close to 100 nm (using naively the cubic lattice picture). In this paper, the authors use this information to justify the possible chain alignment at shear rates lower than $1/\tau_d$, being the reciprocal chain disentanglement time. Based on this picture, they rationalize the occurrence of flow-induced crystallization from unexpectedly low shear rates.

Another example of a striking tTS principle failure is presented in Figure 9E that we have adapted from ref.[179]. This graph shows the Cole-Cole representation of the reduced dynamic viscosity master curves of three crystallizable olefin MBCs of growing molar mass

(from "M01" to "M03") while keeping a similar content in HS ($\approx 25\%$). In this representation, Maxwell fluids exhibit a semi-circular profile, making any deviation from it easy to detect. Note that η'' is systematically lower than η' indicating that all the experiments have been performed well in the flow regime ($G' < G''$). The bottom-left corner concerns the high-frequency regime at which both components of the complex modulus are close to each other. Conversely, the top-right corner rather describes the low frequency window in which tTS failure is expected to happen in microphase separated liquids. Interestingly, while M01 ($M_w = 62\ kg\ mol^{-1}$) does exhibit a semi-circular profile accompanied with a successful application of the tTS, slight deviations appear when passing to M02 ($M_w = 83\ kg\ mol^{-1}$). Increasing further the molar mass in M03 ($M_w = 157\ kg\ mol^{-1}$) has then a dramatic impact on the viscoelastic response that completely deviates from the semi-circular profile and in which tTS clearly fails at low frequencies. Because of a synthesis based on the copolymerization of ethylene and octene, hard and soft segments are poorly defined in these MBCs, making any direct structure-properties relationship difficult to establish. It seems however that longer chains could favor a lower degree of segmentation (*i.e.*, larger blocks in average) enhancing the phase separation in the melt.

Beyond phase separation occurring in MBC melts, rheology can be used to probe more original effects. In Figure 9F, we report from ref.[32], frequency sweep tests measured on a PA1012-PTHF MBC above its melting point. In this case, the samples are heated for two hours at various temperatures (T_{iso}), well above their melting point ($T_m \approx 180\ °C$). To avoid any degradation effect, the measurements are performed under a nitrogen atmosphere. As clearly observed in Figure 9F, the resulting frequency sweeps all exhibit a low-frequency plateau reminiscent of the formation of an elastic network within the MBC melts. While such plateau originated from the phase separation in the previous cases, it stems here from chemical reactions occurring between polyamide-based HSs resulting in the formation of permanent cross-links. Interestingly, the process can be accelerated in a controlled way by increasing the temperature resulting in a higher density of the network, *i.e.*, a higher secondary plateau modulus. While this phenomenon inhibits any possible reshaping of the MBCs, it may be used to provide the material with much stronger non-linear mechanical behavior. In fact, the authors report an increase of the strain and stress at failure by a factor

3 and 2 respectively when passing from an "untreated" MBC to its version pre-heated at $T_{iso} = 270\ ^{\circ}C$. They also point the enhanced PTHF SIC for higher degrees of crosslinking. Contemporaneously, a reduction of the Young modulus is observed, passing from ca. 30 MPa to 20 MPa, corresponding to an expected loss in HS crystallinity.

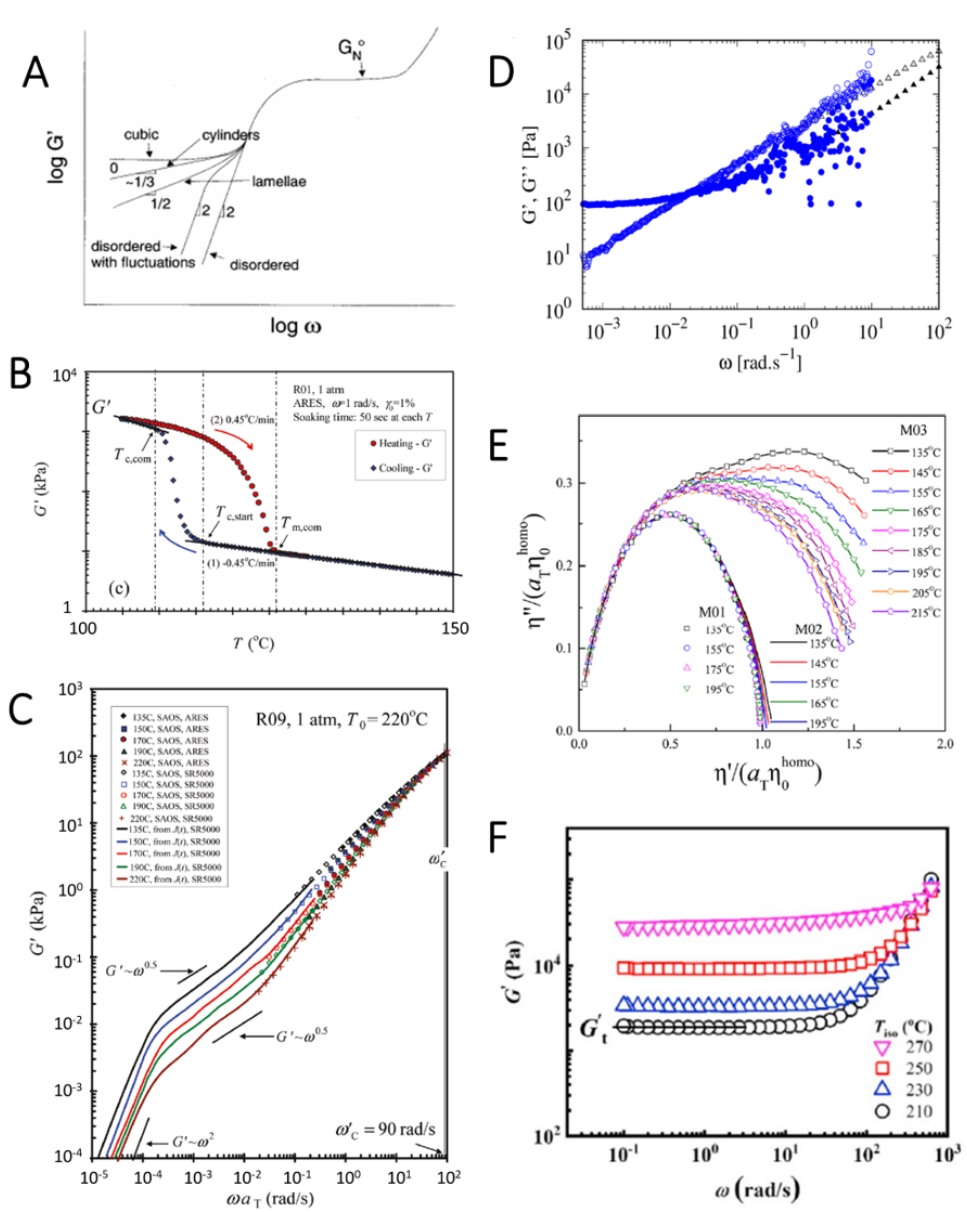

Figure 9: Rheological properties of block-copolymer melts. A) Schematic frequency sweeps of diblock copolymers having different morphologies, adapted from ref.[176]. B) Temperature sweep loop performed on an olefin MBC, adapted from ref.[177]. C) Tentative building of a master curve in a similar olefin MBC, dots and solid lines stand respectively for frequency sweep and creep measurements, adapted from ref.[177]. D) Frequency sweep (black) and creep measurements (blue) performed on a PBT-PTHF MBC, adapted from ref.[178]. E) Cole-Cole representation of master curves measured from three olefin MBCs of growing molecular weight, adapted from ref.[179]. F) Frequency sweep measurements performed on a PA1012-PTHF MBC maintained at various temperatures for 2 hours, adapted from ref.[32].

3.3.2 Non-linear rheology: focus on the Flow-Induced Crystallization

In this last section, we focus our attention on recent works investigating flow induced crystallization (FIC) in semi-crystalline MBCs. FIC must be distinguished from the above-mentioned strain-induced crystallization (SIC) of SS happening in solid-state MBCs at low temperature. In fact, FIC regards the HSs crystallization emerging from liquid MBCs close to their melting point that one can favor upon applying mechanical stress. FIC of polymers is a well explored and "trendy" topic in materials science because it is related to both fundamental understanding of matter and industrial preoccupations related to polymer processing. Recently, it has been the topic of an invited review article by Prof. R. Graham (Univ. of Nottingham, UK) where more than 40 papers published in *Journal of Rheology*, involving mainly homo- (or random co-) polymers, were gathered.[180]. Nevertheless, it seems that very little has been done on MBCs so far. Note however that melt MBCs' manipulation, with no FIC considerations, is well documented. We notably refer the reader to the inspiring work of Bates et al. on pentablock polymers[181] matching industrial needs in the late 90's.[182].

In Figure 10A, we have reported the usual sketch depicting FIC in homopolymers, serving as a visual definition of the phenomenon (adapted from Wang et al.,[183] originally found in ref.[184]). While crystalline lamellae organized into isotropic spherulites emerge from the polymer melt at rest upon cooling, orienting the chains in the macroscopic flow direction results in the formation of a shish-kebab structure. The latter consists of a parallel stack of 2D crystalline lamellae based on folded chain-segments connected with each other through 1D rod-like crystallites containing extended chain-segments. Because of the entropy loss it generates, FIC is expected to increase the crystallization temperature. Regarding the semantics, chain "alignment" occurs when the polymer chains are solicited at a strain rate higher than $1/\tau_d$ whereas chain "stretching" happens for strain rates higher than the reciprocal Rouse time $1/\tau_R$. An analoguous representation of FIC occuring in MBCs by Nebouy et al.[185] is shown in Figure 10B.

The impact of the shear rate on the crystallization of a PBT-PTHF MBC (30 wt.% in HS) is illustrated in Figure 10C where the stress is measured during a start-up shear

experiment in a strain-controlled rheometer (adapted from ref.[178]). The temperature is fixed at 140 $°C$, (*ca.* $T_m - 40$ $°C$), resulting in a crystallization at rest occurring in a few tens of minutes as shown by the small amplitude oscillation shear (SAOS) measurement (dark blue) in *1.* Here, the induction time corresponding to the stress upturn is found to be inversely proportional to the shear rate, indicating that the amount of strain is primarily responsible for the crystallization. The black lines correspond to a model based on the Doi-Edwards equations in which the memory function has been modified so that it depends on the experimental time. More specifically, τ_d is assumed to follow an exponential law coming from the Avrami model in which the crystallization rate k varies as

$$k = \alpha\dot{\gamma}^n + \beta \tag{19}$$

where α is the sensitivity to the shear, $\dot{\gamma}$ is the shear rate, n is the "crystallization mode" related to the geometry of the crystallites and β is the crystallization rate under quiescent conditions. The effect is then confirmed in *2.* by changing the temperature of the experiment. While further heating implies a shorter disentanglement time, *i.e.*, a lower degree of alignment at a given shear rate resulting into a delayed crystallization, the opposite happens upon cooling. Note that the whole sets of black lines in both *1.* and *2.* are respectively fitted to the data with three (shared) parameters only: n, α and β. Remarkably, the latter value was found to be very similar when extracted from isothermal DSC experiments.

In an even more recent paper, we proposed a similar study based on an large amplitude oscillatory shear (LAOS) solicitation.[185] The main results, showing the evolution of the first harmonic dynamic moduli (G_1' and G_1'') as a function of time are presented in Figure 10D, varying either the strain amplitude (γ_{max} in *1.*) or the frequency (ω in *2.*). In both cases, the gelation of the material corresponding roughly to the cross over of the two moduli is found to happen at a shorter time when increasing the maximum shear rate. In fact, plotting the gelation time t_{gel} as a function of the maximum shear rate results in a unique master curve characterized by $t_{gel} \sim (\omega\gamma_{max})^{-1}$, which evidences that the shear rate is primarily controlling the FIC while the strain amplitude and the frequency are secondary. In the same article, the above-mentionned Doi-Edwards inspired model is used to predict rheological responses, providing a good qualitative agreement with the experimental data. More

importantly, using discrete Fourier transform decomposition to access the third harmonic dynamic moduli (G'_3 and G''_3) opens the way to an unprecedented molecular description during the crystallization. In particular, plotting $-G'_3/G'_1$ and G''_3/G''_1 makes emerge different regimes where strain stiffening/softening and shear thickening/thinning can be convincingly related to conformation changes and associations of the MBCs. Finally, SAXS and WAXS are used to emphasize the anisotropy induced by the FIC, revealing notably the radial growth of ribbon-like crystallites such as presented in Figure 10B.

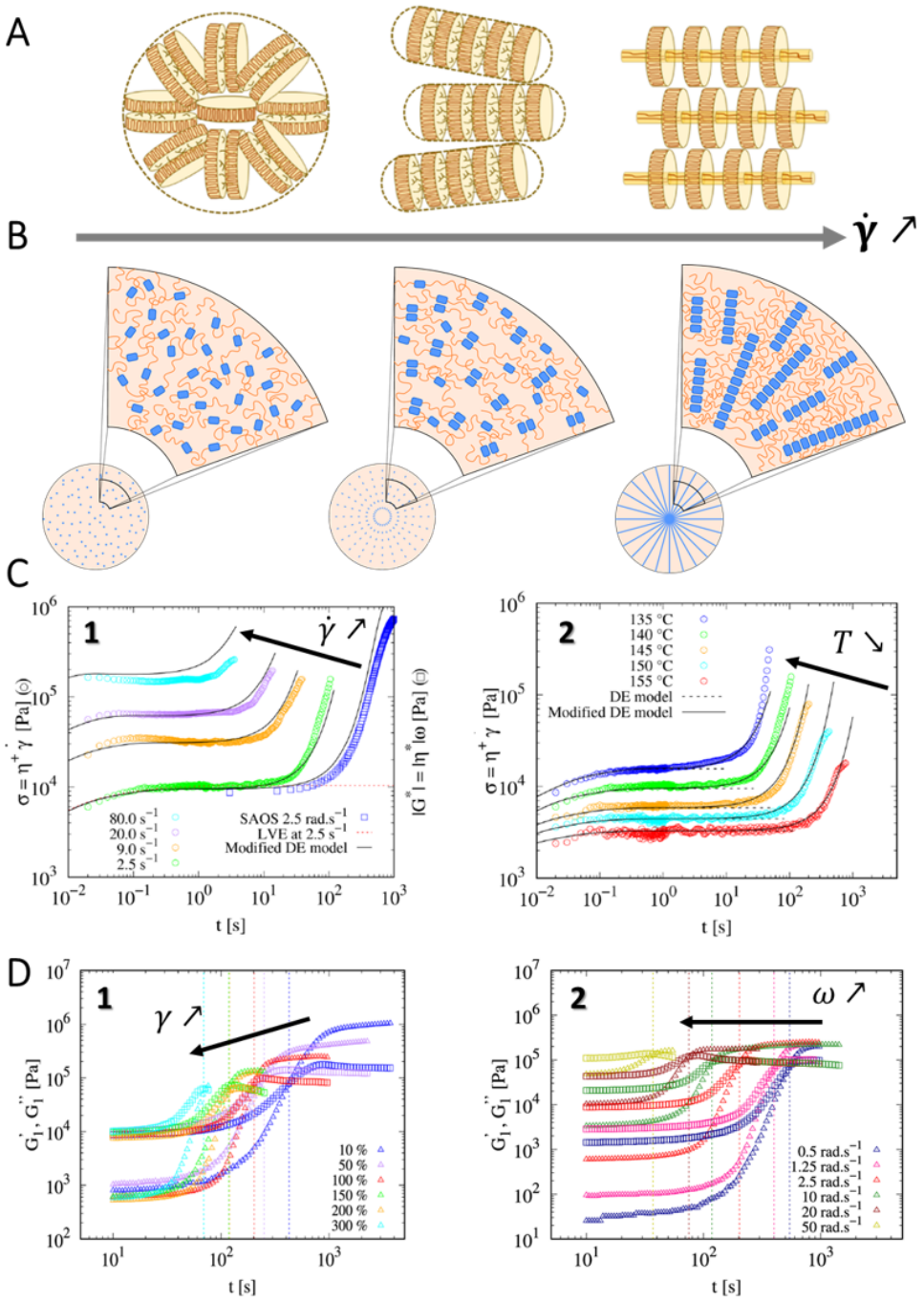

Figure 10: Flow-induced crystallization. A) Schematic representation of a homopolymer crystallized under shear at growing strain rates (left to right), adapted from ref.[183]. B) Analogous picture for MBCs, adapted from ref.[185]. C) Impact of the shear rate (*1.*) and temperature (*2.*) on the FIC of PBT-PTHF MBCs under steady shear, adapted from ref.[178]. D) Impact of the strain amplitude (*1.*) and frequency (*2.*) on the FIC of PBT-PTHF MBCs under LAOS, adapted from ref.[185].

4 Conclusion

Encouraged by the recent examples presented in this review, we prefer to see MBCs as Panacea rather than Pandora's box. In fact, recent progress in chemistry that provides greener solutions coupled with the control of so far (industrially) unexploited physical features such as S/FIC and stimulus-healing capabilities bode well for the future of rubber-like materials. While the first century of polymer science has seen the emergence of a wide variety of elastomers, the second will have undoubtedly to deal with their sustainable production and smarter utilization. To achieve such an ambitious goal, researchers endowed with chemistry, materials science and physics background will necessarily have to propose original solutions to both fundamental questions and industrial requirements beyond the low-cost logic. In fact, the transition from cheap and single use plastics towards more precious and greener materials, including MBCs in a wide range of applications, appears key for a more sustainable development.

Also, the recent advent of computational science, including artificial intelligence, will assuredly have an essential role to play in this adventure. It will serve particularly through its prospective character serving as a guide for chemists and its unique ability to solve the matter at the shortest time- and length-scales. The major challenge that must however be addressed in this field regards the democratization of high computer capabilities. In fact, molecular dynamics simulations are often limited to a few tens of inter-atomic distances, being insufficient to predict macroscopic properties, yet unavoidable in materials science and engineering. A possible solution resides in the more systematic utilization of low computational cost methods such as the ones derived from the self-consistent field theory.

Besides, we are convinced that training (future) researchers in more than one field is key for the development, and any deeper understanding of MBCs. In fact, while writing this article, we realized how fragmented is the polymer science community (between chemical, physical, computational and industrial aspects) and how important it is to "regather" it to achieve veritable research breakthroughs. This fragmentation actually exists beyond disciplinary boundaries, often resulting in the opposition of academic departments dealing with engineering and more fundamental science. In addition, while the research developed by the

industry may have provided some cohesion in the past, the current lack of publication in the open literature appears as another symptom of this chronic fragmentation.

One way to solve this issue may consist of using a common and geometry-oriented language serving to bridge the disciplines. Concretely, this would start with a generalization of the structural notations (see, *e.g.*, topological codes in ref.[186]) and systematic graphical representations of the molecules, too often missing in research papers. An innovative strategy could then rely on investigating molecules of identical architectures but different chemical natures instead of the opposite, which is almost exclusively the case in the MBCs literature. This would serve to identify the role of the sole enthalpic interactions on the microphase separation and the resulting mechanical properties of the materials. Finally, considering the volume fraction of the hard phase rather than its weight fraction should become a habit when rationalizing multiphasic polymers behavior (although weight fraction is certainly relevant from a synthesis point of view).

At last, we hope that the present paper will serve as a mini-guide for the reader, helping him/her to travel into the not so well-defined world of MBCs by addressing frequent questions related to the structure-properties relationship of these fascinating polymers.

REPRINTED FIGURES - RIGHTS

Figure 1

- Reprinted with permission from (Nébouy, Matthias, et al. "Process-oriented structure tuning of PBT/PTHF thermoplastic elastomers." Macromolecules 51.16 (2018): 6291-6302.). Copyright (2018) American Chemical Society.
- Reprinted with permission from (Cao, Yiyu, et al. "Influence of soft block and film thickness on confined morphology of poly (ether-mb-amide) multiblock copolymers." Polymer Crystallization 3.1 (2020): e10100.). Copyright (2020) John Wiley & sons Inc.

Figure 2

- Reprinted with permission from (Zheng, Yi, et al. "Multiblock Copolymers toward Segmentation-Driven Morphological Transition." Macromolecules 53.14 (2020): 5992-6001.). Copyright (2020) American Chemical Society.
- Reprinted with permission from (Vatankhah-Varnosfaderani, Mohammad, et al. "Chameleon-like elastomers with molecularly encoded strain-adaptive stiffening and coloration." Science 359.6383 (2018): 1509-1513.). Copyright (2018) The American Association for the Advancement of Science.

Figure 3

- Reprinted with permission from (Nébouy, Matthias, et al. "Process-oriented structure tuning of PBT/PTHF thermoplastic elastomers." Macromolecules 51.16 (2018): 6291-6302.). Copyright (2018) American Chemical Society.
- Reprinted with permission from (Zhang, Junliang, et al. "Evolution of microphase separation with variations of segments of sequence-controlled multiblock copolymers." Macromolecules 50.18 (2017): 7380-7387.). Copyright (2017) American Chemical Society.
- Reprinted with permission from (Vatankhah-Varnosfaderani, Mohammad, et al. "Chameleon-like elastomers with molecularly encoded strain-adaptive stiffening and coloration." Science 359.6383 (2018): 1509-1513.). Copyright (2018) The American Association for the Advancement of Science.

Figure 4

- Reprinted with permission from (Nébouy, Matthias, et al. "Process-oriented structure tuning of PBT/PTHF thermoplastic elastomers." Macromolecules 51.16 (2018): 6291-6302.). Copyright (2018) American Chemical Society.
- Reprinted with permission from (Candau, Nicolas, et al. "Mechanical reinforcement and memory effect of strain-induced soft segment crystals in thermoplastic polyurethane-urea elastomers." Polymer 223 (2021): 123708.). Copyright (2021) Elsevier.
- Reprinted with permission from (Zhu, Ping, et al. "The segmental responses to orientation and relaxation of thermoplastic poly (ether-ester) elastomer during cyclic deformation: An in-situ WAXD/SAXS study." Polymer 188 (2020): 122120.). Copyright (2020) Elsevier.

Figure 5

- Reprinted with permission from (Heydarnezhad, Hamid Reza, Naser Mohammadi, and Angel Alegria. "Non-Einstein Rheology in Segmented Polyurethane Nanocomposites." Macromolecules 54.6 (2021): 2783-2796.). Copyright (2021) American Chemical Society.
- Reprinted with permission from (de Almeida, André, Matthias Nébouy, and Guilhem P. Baeza. "Bimodal crystallization kinetics of PBT/PTHF segmented block copolymers: Impact of the chain rigidity." Macromolecules 52.3 (2019): 1227-1240.). Copyright (2019) American Chemical Society.
- Reprinted with permission from (Gallu, Raïssa, et al. "Investigating compatibility between TPU and bitumen SARA fractions by means of Hansen solubility parameters and interfacial tension measurements." Construction and Building Materials 289 (2021): 123151.). Copyright (2021) Elsevier.

Figure 6

- Reprinted with permission from (Nébouy, Matthias, et al. "Coarse-grained molecular dynamics modeling of segmented block copolymers: impact of the chain architecture on crystallization and morphology." Macromolecules 53.10 (2020): 3847-3860.). Copyright (2020) American Chemical Society.

- Reprinted with permission from (Spencer, Russell KW, and Mark W. Matsen. "Domain bridging in thermoplastic elastomers of star block copolymer." Macromolecules 50.4 (2017): 1681-1687.). Copyright (2017) American Chemical Society.
- OPEN ACCESS : Jehser, Martin, and Christos N. Likos. "Aggregation shapes of amphiphilic ring polymers: from spherical to toroidal micelles." Colloid and Polymer Science 298.7 (2020): 735-745.

Figure 7

- Reprinted with permission from (Baeza, Guilhem P. "The reinforcement effect in well-defined segmented copolymers: Counting the topological constraints at the mesoscopic scale." Macromolecules 51.5 (2018): 1957-1966.). Copyright (2018) American Chemical Society.
- Reprinted with permission from (Gallu, Raïssa, et al. "On the use of solubility parameters to investigate phase separation-morphology-mechanical behavior relationships of TPU." Polymer 207 (2020): 122882.). Copyright (2020) Elsevier.
- OPEN ACCESS (PhD thesis) : Nebouy, Matthias. Nanostructuration, reinforcement in the rubbery state and flow properties at high shear strain of thermoplastic elastomers: Experiments and modeling. Diss. Université de Lyon, 2020.

Figure 8

- Reprinted with permission from (Xie, Hui, et al. "Effect of Block Number and Weight Fraction on the Structure and Properties of Poly (butylene terephthalate)-block-Poly (tetramethylene oxide) Multiblock Copolymers." Macromolecules 54.6 (2021): 2703-2710.). Copyright (2021) American Chemical Society.
- Reprinted with permission from (Candau, Nicolas, et al. "Mechanical reinforcement and memory effect of strain-induced soft segment crystals in thermoplastic polyurethane-urea elastomers." Polymer 223 (2021): 123708.). Copyright (2021) Elsevier.
- Reprinted with permission from (Sbrescia, Simone, et al. "Morphological origins of temperature and rate dependent mechanical properties of model soft thermoplastic elastomers." Journal of Polymer Science 59.6 (2021): 477-493.). Copyright (2021) Wiley.
- Reprinted with permission from (Aime, Stefano, N. D. Eisenmenger, and T. A. P. Engels. "A model for failure in thermoplastic elastomers based on Eyring kinetics and network connectivity." Journal of Rheology 61.6 (2017): 1329-1342.). Copyright (2017) The Society of Rheology.

Figure 9

- Reprinted with permission from (Park, Heon E., et al. "Rheology and structure of molten, olefin multiblock copolymers." Macromolecules 43.16 (2010): 6789-6799.). Copyright (2010) American Chemical Society.
- Reprinted with permission from (He, Peng, et al. "Mesophase separation and rheology of olefin multiblock copolymers." Macromolecules 47.2 (2014): 807-820.). Copyright (2014) American Chemical Society.
- Reprinted with permission from (Wang, Yu, et al. "Effect of Crosslinking Networks on Strain-induced Crystallization in Polyamide 1012 Multiblock Poly (tetramethylene oxide) Copolymers." Polymer (2021): 123802.). Copyright (2021) Elsevier.
- Reprinted with permission from (Kossuth, M. B., D. C. Morse, and F. S. Bates. "Viscoelastic behavior of cubic phases in block copolymer melts." Journal of Rheology 43.1 (1999): 167-196.). Copyright (1999) The Society of Rheology.
- Reprinted with permission from Nébouy, Matthias, et al. "Modeling shear-induced crystallization in startup flow: The case of segmented copolymers." Journal of Rheology 63.5 (2019): 837-850. Copyright (2019), The Society of Rheology.

Figure 10

- Reprinted with permission from (Wang, Zhen, Zhe Ma, and Liangbin Li. "Flow-induced crystallization of polymers: Molecular and thermodynamic considerations." Macromolecules 49.5 (2016): 1505-1517.). Copyright (2016) American Chemical Society.
- Reprinted with permission from Nébouy, Matthias, et al. "Flow-induced crystallization of a multiblock copolymer under large amplitude oscillatory shear: Experiments and modeling." Journal of Rheology 65.3 (2021): 405-418. Copyright (2021), The Society of Rheology.
- Reprinted with permission from Nébouy, Matthias, et al. "Modeling shear-induced crystallization in startup flow: The case of segmented copolymers." Journal of Rheology 63.5 (2019): 837-850. Copyright (2019), The Society of Rheology.

ACKNOWLEDGMENTS

GPB thanks Matthias Nébouy who greatly contributed to this review article through his Ph.D thesis work (2017-2020), as well as Laurent Chazeau, Florent Dalmas, Julien Morthomas and Claudio Fusco (INSA-Lyon) for enlightening discussions on various aspects regarding block copolymers. GPB also thanks Alexandre Fantou (INSA-Lyon) for editing support.

ORCID

Guilhem P. Baeza : 0000-0002-5142-9670

References

(1) Bates, F. S.; Hillmyer, M. A.; Lodge, T. P.; Bates, C. M.; Delaney, K. T.; Fredrickson, G. H. *Science* **2012**, *336*, 434–440.

(2) Han, C. D.; Kim, J.; Kim, J. K. *Macromolecules* **1989**, *22*, 383–394.

(3) Huy, T. A.; Hai, L. H.; Adhikari, R.; Weidisch, R.; Michler, G. H.; Knoll, K. *Polymer* **2003**, *44*, 1237–1245.

(4) Vinogradov, G. V.; Dreval, V. E.; Malkin, A. Y.; Yanovsky, Y. G.; andE. K. Borisenkova, V. V. B.; Zabugina, M. P.; Plotnikova, E. P.; Sabsai, O. Y. *Rheol. Acta* **1978**, *17*, 258–263.

(5) Adams, J. L.; Graessley, W. W.; Register, R. A. *Macromolecules* **1994**, *27*, 6026–6032.

(6) Hamley, I. W. *Curr. Opin. Colloid Interface Sci.* **2000**, *5*, 342–350.

(7) Van Dijk, M. A.; van den Berg, R. *Macromolecules* **1996**, *28*, 6773–6778.

(8) Van den Berg, R.; de Groot, H.; van Dijk, M.; Denley, D. *Polymer* **1994**, *35*, 5778–5781.

(9) Jangareddy, S.; Sun, T.; Burns, A. B.; Register, R. A. *Macromolecules* **2021**.

(10) Candau, N.; Stoclet, G.; Tahon, J.-F.; Demongeot, A.; Yilgor, E.; Yilgor, I.; Mencelogl u, Y. Z.; Oguz, O. *Polymer* **2021**, 123708.

(11) Kong, X.; Tan, S.; Yang, X.; Li, G.; Zhou, E.; Ma, D. *J. Polym. Sci. Pol. Phys.* **2000**, *38*, 3230–3238.

(12) Hermel, T. J.; Wu, L.; Hahn, S. F.; Lodge, T. P.; Bates, F. S. *Macromolecules* **2002**, *35*, 4685–4689.

(13) Hermel, T. J.; Hahn, S. F.; Chaffin, K. A.; Gerberich, W. W.; Bates, F. S. *Macromolecules* **2003**, *36*, 2190–2193.

(14) Hotta, A.; Cochran, E.; Ruokolainen, J.; Khanna, V.; Fredrickson, G. H.; Kramer, E. J.; Shin, Y.-W.; Shimizu, F.; Cherian, A. E.; Hustad, P. D.; Rose, J. M.; Coates, G. W. *Proc. Natl. Acad. Sci.* **2006**, *103*, 15327–15332.

(15) Vatankhah-Varnosfaderani, M.; Keith, A. N.; Cong, Y.; Liang, H.; Rosenthal, M.; Sztucki, M.; Clair, C.; Magonov, S.; Ivanov, D. A.; Dobrynin, A. V., et al. *Science* **2018**, *359*, 1509–1513.

(16) Bui, R.; Brook, M. A. *Green Chemistry* **2021**.

(17) Auriemma, F.; Di Girolamo, R.; Urciuoli, G.; Caputo, M. R.; De Rosa, C.; Scoti, M.; Malafronte, A.; Cipullo, R.; Busico, V.; Grizzuti, N., et al. *Polymer* **2020**, *193*, 122347.

(18) Bandara, U.; Dröscher, M. *Colloid Polym. Sci.* **1983**, *261*, 26–39.

(19) Wegner, G.; Fuji, T.; Meyer, W.; Lieser, G. *Die Angewandte Makromolekulare Chemie* **1978**, *74*, 295–316.

(20) Zhu, P.; Zhou, C.; Dong, X.; Sauer, B. B.; Lai, Y.; Wang, D. *Polymer* **2020**, *188*, 122120.

(21) Sauer, B. B.; Kampert, W. G. *J. Appl. Polym. Sci.* **2020**, 49315.

(22) Gaymans, R. J.; de Haan, J. L. *Polymer* **1993**, *34*, 4360–4364.

(23) Sharma, A.; Baeza, G. P.; Imperiali, L.; Appel, W. P.; Fitié, C.; Poel, G. V.; van Ruymbeke, E. *Polym. Int.* **2018**, *68*, 283–293.

(24) Biemond, G.; Feijen, J.; Gaymans, R. *Polym. Eng. Sci.* **2008**, *48*, 1389–1400.

(25) Biemond, G. J. E.; Feijen, J.; Gaymans, R. J. *J. Mater. Sci.* **2008**, *43*, 3689–3696.

(26) Niesten, M.; Feijen, J.; Gaymans, R. *Polymer* **2000**, *41*, 8487–8500.

(27) Arun, A.; Gaymans, R. J. *Macromol. Chem. Phys.* **2008**, *209*, 854–863.

(28) Bai, L.; Hong, Z.; Wang, D.; Li, J.; Wang, X.; Pan, G.; Li, L.; Li, X. *Polymer* **2010**, *51*, 5604–5611.

(29) Baeza, G. P.; Sharma, A.; Louhichi, A.; Imperiali, L.; Appel, W. P.; Fitié, C. F.; Lettinga, M. P.; Ruymbeke, E. V.; Vlassopoulos, D. *Polymer* **2016**, *107*, 89–101.

(30) Krijgsman, J.; Husken, D.; Gaymans, R. *Polymer* **2003**, *44*, 7573–7588.

(31) Sijbrandi, N. J.; Kimenai, A. J.; Mes, E. P. C.; Broos, R.; Bar, G.; Rosenthal, M.; Odarchenko, Y.; Ivanov, D. A.; Dijkstra, P. J.; Feijen, J. *Macromolecules* **2012**, *45*, 3948–3961.

(32) Wang, Y.; Zhu, P.; Lai, Y.; Wang, L.; Wang, D.; Dong, X. *Polymer* **2021**, 123802.

(33) Miller, J. A.; ans Kirk K. S. Hwang, S. B. L.; Wu, K. S.; Gibson, P. E.; Cooper, S. L. *Macromolecules* **1985**, *18*, 32–44.

(34) Petrovic, Z. S. *J. Polym. Sci. Pol. Phys.* **1989**, *27*, 545–560.

(35) Nichetti, D.; Grizzuti, N. *Polym. Eng. Sci.* **2004**, *44*, 1514–1521.

(36) Oguz, O.; Koutsoumpis, S. A.; Simsek, E.; Yilgor, E.; Yilgor, I.; Pissis, P.; Menceloglu, Y. Z. *RSC Adv.* **2017**, *7*, 40745–40754.

(37) Qi, H.; Boyce, M. *Mech. Mater.* **2005**, *37*, 817–839.

(38) Fragiadakis, D.; Runt, J. *Macromolecules* **2013**, *46*, 4184–4190.

(39) Nikonorova, N. A.; Didenko, A. L.; Kudryavtsev, V. V.; Castro, R. A. *J. Non-Cryst. Solids* **2016**, *447*, 117–122.

(40) Heydarnezhad, H. R.; Mohammadi, N.; Arbe, A.; Alegria, A. *Macromolecules* **2020**, *53*, 5381–5398.

(41) Heydarnezhad, H. R.; Mohammadi, N.; Alegria, A. *Macromolecules* **2021**.

(42) Viviani, M.; Fluitman, S. P.; Loos, K.; Portale, G. *Polymer Chemistry* **2021**.

(43) Ruzette, A.-V.; Leibler, L. *Nature materials* **2005**, *4*, 19–31.

(44) Dobrynin, A. V.; Erukhimovich, I. Y. *Macromolecules* **1993**, *26*, 276–281.

(45) Benoit, H.; Hadziioannou, G. *Macromolecules* **1988**, *21*, 1449–1464.

(46) Borisov, O. V.; Zhulina, E. B. *Macromolecules* **2005**, *38*, 2506–2514.

(47) Ellis, P. **2021**.

(48) Panigrahi, R.; Zarek, M.; Sharma, V.; Cohn, D.; Ramanujan, R. V. *Macromolecular Chemistry and Physics* **2019**, *220*, 1900168.

(49) Ahmed, A. S.; Ramanujan, R. V. *Scientific reports* **2015**, *5*, 1–10.

(50) Amin, S.; Amin, M. *Rev. Adv. Mater. Sci.* **2011**, *29*, 15–30.

(51) Michelin The VISION Concept Accessed Jan. 26, 2021, https://www.michelin.com/en/innovation/vision-concept/.

(52) Michelin UPTIS unveiled to the public Accessed Jan. 26, 2021, https://www.michelin.com/en/news/uptis-unveiled-to-the-public/.

(53) Lu, X.; Isacsson, U. *Polym. Test.* **2001**, *20*, 77–86.

(54) Gallu, R.; Méchin, F.; Dalmas, F.; Gérard, J.-F.; Perrin, R.; Loup, F. *Polymer* **2020**, *207*, 122882.

(55) Bae, D.; Moon, M. J.; Shon, M. Y.; Oh, S. T.; Kim, G. N.; Yun, D. W. *The Journal of Adhesion* **2017**, *93*, 964–979.

(56) Salimi, S.; Babra, T. S.; Dines, G. S.; Baskerville, S. W.; Hayes, W.; Greenland, B. W. *European Polymer Journal* **2019**, *121*, 109264.

(57) Kishi, H.; Kuwata, M.; Matsuda, S.; Asami, T.; Murakami, A. *Composites Science and Technology* **2004**, *64*, 2517–2523.

(58) Li, H.; White, J. L. *Polymer Engineering & Science* **2000**, *40*, 917–928.

(59) Huang, W.; Pan, Q.; Qi, H.; Li, X.; Tu, Y.; Li, C. Y. *Polymer* **2017**, *128*, 188–199.

(60) Eastwood, E.; Dadmun, M. *Macromolecules* **2002**, *35*, 5069–5077.

(61) Zhou, J.; Xu, X.; Xin, Y.; Lubineau, G. *Advanced Functional Materials* **2018**, *28*, 1705591.

(62) Probst, H.; Katzer, K.; Nocke, A.; Hickmann, R.; Zimmermann, M.; Cherif, C. *Polymers* **2021**, *13*, 590.

(63) Avient https://omnexus.specialchem.com/news/product-news/avient-thermoplastic-elastomers-microbial-additives-000224679.

(64) Drobny, J. G., *Handbook of Thermoplastic Elastomers*; Elsevier Science: 2007.

(65) Jeon, S. H.; Jeong, J. E.; Kim, S.; Jeon, S.; Choung, J. W.; Kim, I. *Polymers* **2021**, *13*, 525.

(66) McMullin, E.; Rebar, H. T.; Mather, P. T. *Macromolecules* **2016**, *49*, 3769–3779.

(67) Nakayama, Y.; Aihara, K.; Yamanishi, H.; Fukuoka, H.; Tanaka, R.; Cai, Z.; Shiono, T. *Journal of Polymer Science Part A: Polymer Chemistry* **2015**, *53*, 489–495.

(68) Chen, X.; Zhou, Z.; Zhang, H.; Mao, Y.; Luo, Z.; Li, X.; Sha, Y. *Macromolecular Chemistry and Physics* **2021**, 2100055.

(69) Gaymans, R. J. *Prog. Polym. Sci.* **2011**, *36*, 713–748.

(70) Zheng, Y.; Weng, C.; Cheng, C.; Zhao, J.; Yang, R.; Zhang, Q.; Ding, M.; Tan, H.; Fu, Q. *Macromolecules* **2020**, *53*, 5992–6001.

(71) Onoda, M.; Ueki, T.; Shibayama, M.; Yoshida, R. *Scientific reports* **2015**, *5*, 1–9.

(72) Leibler, L. *Macromolecules* **1980**, *13*, 1602–1617.

(73) Matsen, M. W.; Schick, M. *Macromolecules* **1994**, *27*, 7157–7163.

(74) Seguela, R. *Journal of Polymer Science Part B: Polymer Physics* **2005**, *43*, 1729–1748.

(75) Rowan, S. J. Happy 100th Anniversary to Polymer Science and Engineering, 2020.

(76) Callaway, E. *Nature* **2020**.

(77) Krause, S. *Macromolecules* **1970**, *3*, 84–86.

(78) Matsen, M. W. *Journal of Physics: Condensed Matter* **2001**, *14*, R21.

(79) Fredrickson, G. H.; Ganesan, V.; Drolet, F. *Macromolecules* **2002**, *35*, 16–39.

(80) Arora, A.; Qin, J.; Morse, D. C.; Delaney, K. T.; Fredrickson, G. H.; Bates, F. S.; Dorfman, K. D. *Macromolecules* **2016**, *49*, 4675–4690.

(81) Spencer, R. K.; Matsen, M. W. *Macromolecules* **2017**, *50*, 1681–1687.

(82) Niesten, M.; Gaymans, R. *Polymer* **2001**, *42*, 6199–6207.

(83) Biemond, G. J. E.; Feijen, J.; Gaymans, R. J. *Macromol. Mater. Eng.* **2009**, *294*, 492–501.

(84) Grest, G. S.; Kremer, K. *Phys. Rev. A* **1986**, *33*, 3628–3631.

(85) Kremer, K.; Grest, G. S. *J. Chem. Phys.* **1990**, *92*, 5057–5086.

(86) Leibler, L.; Rubinstein, M.; Colby, R. H. *Macromolecules* **1991**, *24*, 4701–4707.

(87) Simonin, L.; Falco, G.; Pensec, S.; Dalmas, F.; Chenal, J.-M.; Ganachaud, F.; Marcellan, A.; Chazeau, L.; Bouteiller, L. *Macromolecules* **2021**, *54*, 888–895.

(88) Sbrescia, S.; Ju, J.; Engels, T.; Van Ruymbeke, E.; Seitz, M. *Journal of Polymer Science* **2021**, *59*, 477–493.

(89) Cui, Z.; Brinson, L. C. *Phys. Rev. E* **2013**, *88*, 1539–3755.

(90) Shabbir, A.; Huang, Q.; Baeza, G. P.; Vlassopoulos, D.; Chen, Q.; Colby, R. H.; Alvarez, N. J.; Hassager, O. *J. Rheol.* **2017**, *61*, 1279–1289.

(91) Flory, P. J. *The Journal of chemical physics* **1942**, *10*, 51–61.

(92) Huggins, M. L. *The Journal of Physical Chemistry* **1942**, *46*, 151–158.

(93) Meier, D. J. *J. Polymer Sci. Part C* **1969**, *26*, 81–88.

(94) Helfand, E. *Macromolecules* **1975**, *8*, 552–556.

(95) Fredrickson, G. H.; Liu, A. J.; Bates, F. S. *Macromolecules* **1994**, *27*, 2503–2511.

(96) Fredrickson, G. H.; Helfand, E. *J. Chem. Phys.* **1987**, *87*, 697–705.

(97) Bates, F. S.; Fredrickson, G. H. *Phys. Today* **1999**, *52*, 32–38.

(98) Bates, F. S.; Fredrickson, G. H. *Annu. Rev. Phys. Chem.* **1990**, *41*, 525–575.

(99) Mikhailov, I. V.; Leermakers, F. A.; Darinskii, A. A.; Zhulina, E. B.; Borisov, O. V. *Macromolecules* **2021**.

(100) Lee, I.; Panthani, T. R.; Bates, F. S. *Macromolecules* **2013**, *46*, 7387–7398.

(101) Lee, I.; Bates, F. S. *Macromolecules* **2013**, *46*, 4529–4539.

(102) Spontak, R. J.; Smith, S. D. *J. Polym. Sci. Pol. Phys.* **2001**, *39*, 947–955.

(103) Balazs, A. C.; Singh, C.; Zhulina, E. *Macromolecules* **1998**, *31*, 8370–8381.

(104) Ceniceros, H. D.; Fredrickson, G. H. *Multiscale Modeling & Simulation* **2004**, *2*, 452–474.

(105) Loo, Y.-L.; Register, R. A.; Ryan, A. J. *Macromolecules* **2002**, *35*, 2365–2374.

(106) He, W.-N.; Xu, J.-T. *Prog. Polym. Sci.* **2012**, *37*, 1350–1400.

(107) Rangarajan, P.; Register, R. A.; Fetters, L. J. *Macromolecules* **1993**, *26*, 4640–4645.

(108) Koo, C. M.; Hillmyer, M. A.; Bates, F. S. *Macromolecules* **2006**, *39*, 667–677.

(109) Nébouy, M.; de Almeida, A.; Brottet, S.; Baeza, G. P. *Macromolecules* **2018**, *51*, 6291–6302.

(110) Cao, Y.; Zhu, P.; Zhou, Y.; Wang, D.; Dong, X. *Polym. Crystallization* **2020**, *3*, e10100.

(111) Cao, Y.; Zhu, P.; Wang, Z.; Zhou, Y.; Chen, H.; Müller, A. J.; Wang, D.; Dong, X. *Polymer Crystallization* **2018**, *1*, e10012.

(112) Panthani, T. R.; Bates, F. S. *Macromolecules* **2015**, *48*, 4529–4540.

(113) Zhang, J.; Deubler, R.; Hartlieb, M.; Martin, L.; Tanaka, J.; Patyukova, E.; Topham, P. D.; Schacher, F. H.; Perrier, S. *Macromolecules* **2017**, *50*, 7380–7387.

(114) Gallu, R.; Méchin, F.; Dalmas, F.; Gérard, J.-F.; Perrin, R.; Loup, F. *Construction and Building Materials* **2021**, *289*, 123151.

(115) Schön, P.; Bagdi, K.; Molnár, K.; Markus, P.; Pukánszky, B.; Vancso, G. J. *European Polymer Journal* **2011**, *47*, 692–698.

(116) De Almeida, A.; Nébouy, M.; Baeza, G. P. *Macromolecules* **2019**, *52*, 1227–1240.

(117) Posselt, D.; Zhang, J.; Smilgies, D.-M.; Berezkin, A. V.; Potemkin, I. I.; Papadakis, C. M. *Progress in polymer science* **2017**, *66*, 80–115.

(118) Jung, F. A.; Posselt, D.; Smilgies, D.-M.; Panteli, P. A.; Tsitsilianis, C.; Patrickios, C. S.; Papadakis, C. M. *Macromolecules* **2020**, *53*, 6255–6266.

(119) Berezkin, A. V.; Jung, F.; Posselt, D.; Smilgies, D. M.; Papadakis, C. M. *ACS Appl. Mater. Interfaces* **2017**, *9*, 31291–31301.

(120) Hamley, I. W.; Castelletto, V. *Progress in polymer science* **2004**, *29*, 909–948.

(121) Zhu, P.; Zhou, C.; Wang, Y.; Sauer, B.; Hu, W.; Dong, X.; Wang, D. *ACS Applied Polymer Materials* **2021**.

(122) Meyer, H. W.; Schneider, H.; Saalwächter, K. *Polymer journal* **2012**, *44*, 748–756.

(123) Schneider, H.; Saalwächter, K.; Roos, M. *Macromolecules* **2017**, *50*, 8598–8610.

(124) Roos, M.; Schäler, K.; Seidlitz, A.; Thurn-Albrecht, T.; Saalwächter, K. *Colloid and Polymer Science* **2014**, *292*, 1825–1839.

(125) Saalwächter, K.; Thomann, Y.; Hasenhindl, A.; Schneider, H. *Macromolecules* **2008**, *41*, 9187–9191.

(126) Schäler, K.; Roos, M.; Micke, P.; Golitsyn, Y.; Seidlitz, A.; Thurn-Albrecht, T.; Schneider, H.; Hempel, G.; Saalwächter, K. *Solid state nuclear magnetic resonance* **2015**, *72*, 50–63.

(127) Clauss, J.; Schmidt-Rohr, K.; Spiess, H. W. *Acta Polymerica* **1993**, *44*, 1–17.

(128) Heydarnezhad, H. R.; Mohammadi, N.; Arbe, A.; Alegria, A. *Macromolecules* **2020**, *53*, 5381–5398.

(129) Abbott, S.; Hansen, C. M., *Hansen solubility parameters in practice*; Hansen-Solubility: 2008.

(130) Gallu, R.; Méchin, F.; Dalmas, F.; Gérard, J.-F.; Perrin, R.; Loup, F. *Construction and Building Materials* **2020**, *259*, 120404.

(131) Everaers, R.; Karimi-Varzaneh, H. A.; Fleck, F.; Hojdis, N.; Svaneborg, C. *Macromolecules* **2020**, *53*, 1901–1916.

(132) Svaneborg, C.; Karimi-Varzaneh, H. A.; Hojdis, N.; Fleck, F.; Everaers, R. **2018**, arXiv:1808.03509 [cond-mat.soft].

(133) Qin, J.; Luo, W.; Li, M.; Chen, P.; Wang, S.; Ren, S.; Han, D.; Xiao, M.; Meng, Y. *ACS Sustainable Chemistry & Engineering* **2017**, *5*, 5922–5930.

(134) Nébouy, M.; Morthomas, J.; Fusco, C.; Baeza, G. P.; Chazeau, L. *Macromolecules* **2020**, *53*, 3847–3860.

(135) Jaramillo-Cano, D.; Formanek, M.; Likos, C. N.; Camargo, M. *The Journal of Physical Chemistry B* **2018**, *122*, 4149–4158.

(136) Goodson, A. D.; Troxler, J. E.; Rick, M. S.; Ashbaugh, H. S.; Albert, J. N. *Macromolecules* **2019**, *52*, 9389–9397.

(137) Jehser, M.; Likos, C. N. *Colloid and Polymer Science* **2020**, *298*, 735–745.

(138) Peters, A. J.; Lawson, R. A.; Nation, B. D.; Ludovice, P. J.; Henderson, C. L. *Nanotechnology* **2015**, *26*, 385301.

(139) Morthomas, J.; Fusco, C.; Zhai, Z.; Lame, O.; Perez, M. *Phys. Rev. E* **2017**, *96*, 052502.

(140) Zhai, Z.; Fusco, C.; Morthomas, J.; Perez, M.; Lame, O. *ACS Nano* **2019**, *13*, 11310–11319.

(141) Parker, A. J.; Rottler, J. *ACS Macro Letters* **2017**, *6*, 786–790.

(142) Jabbari-Farouji, S.; Lame, O.; Perez, M.; Rottler, J.; Barrat, J.-L. *Phys. Rev. Lett.* **2017**, *118*, 217802.

(143) Kröger, M. *Comput. Phys. Commun.* **2005**, *168*, 209–232.

(144) Puskas, J.; Antony, P.; El Fray, M.; Altstädt, V. *European Polymer Journal* **2003**, *39*, 2041–2049.

(145) Burns, A. B.; Register, R. A. *Macromolecules* **2016**, *49*, 9521–9530.

(146) Kapnistos, M.; Lang, M.; Vlassopoulos, D.; Pyckhout-Hintzen, W.; Richter, D.; Cho, D.; Chang, T.; Rubinstein, M. *Nature materials* **2008**, *7*, 997–1002.

(147) Hou, J.-X. *Journal of Rheology* **2020**, *64*, 1315–1324.

(148) Tsalikis, D. G.; Mavrantzas, V. G.; Vlassopoulos, D. *ACS Macro Letters* **2016**, *5*, 755–760.

(149) Rubinstein, M.; Colby, R. H., *Polymer Physics*; Oxford University Press, United Kingdom: 2003.

(150) Doi, M.; Edwards, S. F. *J. Chem. Soc., Faraday Trans. 2* **1978**, *74*, 1789–1801.

(151) Fetters, L. J.; Lohse, D. J.; Colby, R. H., *Chain Dimensions and Entanglement Spacings*; Springer: New York: 2007.

(152) Einstein, A. *Ann. d. Phys* **1905**, *17*, 1.

(153) Smallwood, H. M. *J. Appl. Phys.* **1944**, *15*, 758–766.

(154) Guth, E. *Rubber Chem. and Technol.* **1945**, *18*, 596–604.

(155) Batchelor, G.; Green, J. *Journal of Fluid Mechanics* **1972**, *56*, 401–427.

(156) Song, Y.; Zheng, Q. *Progress in Materials Science* **2016**, *84*, 1–58.

(157) Mujtaba, A.; Keller, M.; Ilisch, S.; Radusch, H.-J.; Thurn-Albrecht, T.; Saalwächter, K.; Beiner, M. *Macromolecules* **2012**, *45*, 6504–6515.

(158) Baeza, G. P.; Genix, A.-C.; Degrandcourt, C.; Petitjean, L.; Gummel, J.; Couty, M.; Oberdisse, J. *Macromolecules* **2012**, *46*, 317–329.

(159) Payne, A. R. *J. Appl. Polym. Sci.* **1962**, *6*, 57–63.

(160) Takayanagi, M.; Uemura, S.; Minami, S. In *J. Polym. Sci. Part C: Polym. Symp.* 1964; Vol. 5, pp 113–122.

(161) Humbert, S.; Lame, O.; Séguéla, R.; Vigier, G. *Polymer* **2011**, *52*, 4899–4909.

(162) Seguela, R. *J. Polym. Sci., Part B: Polym. Phys.* **2005**, *43*, 1729–1748.

(163) Krigbaum, W.; Roe, R.-J.; Smith Jr, K. *Polymer* **1964**, *5*, 533–542.

(164) Zhu, L.-L.; Wegner, G.; Bandara, U. *Macromol. Chem.* **1981**, *182*, 3639–3651.

(165) Nébouy, M.; Louhichi, A.; Baeza, G. P. *Journal of Polymer Engineering* **2020**, *40*, 715–726.

(166) Baeza, G. P. *Macromolecules* **2018**, *51*, 1957–1966.

(167) Van der Schuur, M.; Gaymans, R. J. *J. Polym. Sci. Pol. Chem.* **2006**, *44*, 4769–4781.

(168) Husken, D.; Feijen, J.; Gaymans, R. J. *J. Polym. Sci., Part A: Polym. Chem.* **2007**, *45*, 4522–4535.

(169) Versteegen, R. M.; Kleppinger, R.; Sijbesma, R. P.; Meijer, E. *Macromolecules* **2006**, *39*, 772–783.

(170) Lee, H. S.; Park, H. D.; Cho, C. K. *J. Polym. Sci. Pol. Phys.* **2000**, *77*, 699–709.

(171) Nebouy, M. Nanostructuration, reinforcement in the rubbery state and flow properties at high shear strain of thermoplastic elastomers: Experiments and modeling, Ph.D. Thesis, Université de Lyon, 2020.

(172) Popov, I.; Carroll, B.; Bocharova, V.; Genix, A.-C.; Cheng, S.; Khamzin, A.; Kisliuk, A.; Sokolov, A. P. *Macromolecules* **2020**, *53*, 4126–4135.

(173) Baeza, G. P.; Dessi, C.; Costanzo, S.; Zhao, D.; Gong, S.; Alegria, A.; Colby, R. H.; Rubinstein, M.; Vlassopoulos, D.; Kumar, S. K. *Nature Communications* **2016**, *7*, 11368.

(174) Xie, H.; Lu, H.; Zhang, Z.; Li, X.; Yang, X.; Tu, Y. *Macromolecules* **2021**, *54*, 2703–2710.

(175) Aime, S.; Eisenmenger, N. D.; Engels, T. A. P. *J. Rheol.* **2017**, *61*, 1329–1342.

(176) Kossuth, M.; Morse, D.; Bates, F. *Journal of Rheology* **1999**, *43*, 167–196.

(177) Park, H. E.; Dealy, J. M.; Marchand, G. R.; Wang, J.; Li, S.; Register, R. A. *Macromolecules* **2010**, *43*, 6789–6799.

(178) Nébouy, M.; de Almeida, A.; Chazeau, L.; Baeza, G. P. *J. Rheol.* **2019**, *63*, 837–850.

(179) He, P.; Shen, W.; Yu, W.; Zhou, C. *Macromolecules* **2014**, *47*, 807–820.

(180) Graham, R. https://sor.scitation.org/toc/jor/collection/10.1122/jor.2019.FIC2019.issue-1.

(181) Bates, F. S.; Fredrickson, G. H.; Hucul, D.; Hahn, S. F. *American Institute of Chemical Engineers. AIChE Journal* **2001**, *47*, 762.

(182) Vigild, M. E.; Chu, C.; Sugiyama, M.; Chaffin, K.; Bates, F. *Macromolecules* **2001**, *34*, 951–964.

(183) Wang, Z.; Ma, Z.; Li, L. *Macromolecules* **2016**, *49*, 1505–1517.

(184) Swartjes, F. H. M.; Peters, G. W.; Rastogi, S.; Meijer, H. E. *International Polymer Processing* **2003**, *18*, 53–66.

(185) Nébouy, M.; Chazeau, L.; Morthomas, J.; Fusco, C.; Dieudonné-George, P.; Baeza, G. P. *Journal of Rheology* **2021**, *65*, 405–418.

(186) Gu, Y.; Zhao, J.; Johnson, J. A. *Trends in Chemistry* **2019**, *1*, 318–334.

About the author

Guilhem P. Baeza obtained a joint Master degree in materials science and engineering from Politecnico di Torino (IT) and Polytech' Montpellier (FR) in 2010. He received his Ph.D in 2013 from the University of Montpellier for his work on simplified industrial nanocomposites in collaboration with *Michelin*, under the supervision of Dr. J. Oberdisse and Dr. M. Couty. After a post-doc at FORTH, Heraklion (GR) in the group of Prof. D. Vlassopoulos, and a short stay at the University of Leeds (UK), he started to work in 2016 as professor assistant at INSA-Lyon (FR). His research focuses on the structure-properties relationship of nanostructured polymer based materials.

G.P. Baeza, INSA-Lyon, 2016